Science of Remote Sensing 10 (2024) 100161

Contents lists available at ScienceDirect

Science of Remote Sensing

journal homepage: www.sciencedirect.com/journal/science-of-remote-sensing

Evaluation of GEDI footprint level biomass models in Southern African Savannas using airborne LiDAR and field measurements

Xiaoxuan Li [a], Konrad Wessels [a,*], John Armston [b], Laura Duncanson [b], Mikhail Urbazaev [b], Laven Naidoo [c,d], Renaud Mathieu [e], Russell Main [f]

[a] Department of Geography and Geoinformation Science, George Mason University, Fairfax, 22030 VA, United States
[b] Department of Geographical Sciences, University of Maryland College Park, College Park, 20742 MD, United States
[c] Gauteng City-Region Observatory (GCRO), Private Bag 3, Wits, 2050, Johannesburg, South Africa
[d] Department of Geography, GeoInformatics & Meteorology Geography, University of Pretoria, Pretoria, 0083, South Africa
[e] IRRI AFRICA C/O ILRI, Nairobi, 00100, Kenya
[f] Precision Agriculture Group, Advanced Agriculture and Food Cluster, Council for Scientific and Industrial Research, Pretoria, South Africa

ARTICLE INFO

Keywords:
LiDAR
GEDI
Aboveground biomass density
Validation
Savannas
Africa

ABSTRACT

Savannas cover more than 20% of the Earth and account for the third largest stock of global aboveground biomass yet estimates of their above ground biomass density (AGBD) are very inaccurate. The Global Ecosystem Dynamic Investigation (GEDI) sensor provides near-global full-waveform LiDAR data with 25 m footprints, from which various structural metrics are derived that are used to predict footprint level AGBD. The current GEDI L4A AGBD product uses a comprehensive Forest Structure and Biomass Database (FSBD) to develop models for specific plant functional types and geographic regions, but southern African savannas have been underrepresented in the reference data. The objectives of this study were to (i) validate GEDI L4A AGBD in South African savannas using field measurements and ALS datasets and (ii) develop and evaluate local GEDI footprint-level AGBD estimates from multiple L2A and L2B metrics. The local GEDI AGBD models outperformed GEDI L4A AGBD ($R^2 = 0.42$, RMSE = 12 Mg/ha, %RMSE = 79.5%) with higher R^2 and smaller error measures. The local GEDI AGBD using a random forest model (RF) had the highest R^2 of 0.71 and lowest %RMSE of 53.3%, while the generalized linear model (GLM) results provided the lowest Relative Mean Systematic Deviation (RMSD) of 9.2%, which was half that of RF model. L4A significantly underestimated AGBD with an RMSD up to −37%. This highlights the importance and benefits of local calibration of biomass models to unlock the full potential of GEDI metrics for estimating AGBD. The field and ALS data have subsequently been contributed to the GEDI FSBD and should be used in calibration of future versions of GEDI L4A AGBD product. This research paves the way for the integration of the local GEDI AGBD estimates with other sensors, notable the eminent NISAR mission, to derive regional to global gridded AGBD products that will enable the monitoring of savanna carbon stocks.

1. Introduction

Savannas are mixed woodland-grassland ecosystems characterized by a continuous grass layer and a discontinuous tree layer (Scholes and Archer, 1997). Savannas cover more than 20% of the Earth and account for the third largest stock of global aboveground biomass (AGB) (Scharlemann et al., 2014). Global maps of carbon stocks greatly underestimate the biomass of woody vegetation outside of closed canopy forests in Africa (Bastin et al., 2017; Skole et al., 2021). Savannas are highly heterogeneous with great variability in the horizontal and vertical structure of woody vegetation that challenges remotely sensed estimates of biomass estimates with large errors (relative Root Mean Square Error - rRMSE) of 50–100% in regions with AGB density (AGBD) < 60 Mg/ha (Rodríguez-Veiga et al., 2019). A recent comparison of state-of-the-art AGBD maps derived using remote sensing or ecosystem models (Bouvet et al., 2018; Hanan et al., 2020; Sitch et al., 2015) in the drylands of sub-Saharan Africa demonstrated that their AGBD predictions differ by up to 250% (Tucker et al., 2023). Gridded products of AGBD furthermore require sufficiently fine spatial scales and adequate levels of accuracy to capture changes in savanna biomass caused by anthropogenic drivers including debushing, fuelwood extraction and charcoal production (Swemmer et al., 2019; Twine and Holdo, 2016;

* Corresponding author.
E-mail address: kwessel4@gmu.edu (K. Wessels).

https://doi.org/10.1016/j.srs.2024.100161
Received 30 January 2024; Received in revised form 12 August 2024; Accepted 4 September 2024
Available online 7 September 2024

Wessels et al., 2013, 2019), as well as natural drivers such as wildfire, shrub encroachment due to CO_2 increases and elephant impacts (Asner et al., 2016; Mograbi et al., 2015, 2017; Sankaran et al., 2008; Smit et al., 2010, 2016; Wigley et al., 2010; Venter et al., 2018). Accurate estimates of AGBD are furthermore essential to predicting forest carbon stocks (Coomes et al., 2017) or large-scale afforestation programs (O'Connor and Ford, 2014) aimed at greenhouse gas and climate change mitigation through programs such as the United Nations' Reducing Emissions from Deforestation and Degradation-plus (REDD +) and commitments following the Paris Agreement the United Nations Framework Convention on Climate Change (UNFCCC) (Leitold et al., 2015; Mitchell et al., 2017; Skole et al., 2021).

Forest AGB is defined as "dry-weight of the standing live or dead woody component of aboveground vegetation" (Ashton et al., 2012; Bombelli et al., 2009). AGB has been recognized as a Global Climate Observing System (GCOS) Essential Climate Variable (ECV) and a critical input to the United Nations' REDD + program (Coops et al., 2021; Duncanson et al., 2019; Herold et al., 2019). Destructive harvesting of trees for biomass estimation is expensive and impractical. Instead, statistical models (i.e. allometric models) are used to estimate individual tree AGB from non-destructive measurements such as tree crown diameter, tree height, diameter at breast height (DBH), wood density (WD), and stem diameter (SD), etc. (Asner and Mascaro, 2014; Chave et al., 2005; Coomes et al., 2017; Duncanson et al., 2021; Eisfelder et al., 2012; Lu et al., 2016). The individual tree-level AGB estimates are typically summed within a plot with a specific area to calculate plot-level aboveground biomass density (AGBD) that quantifies the amount of AGB per unit area and is expressed in megagrams per hectare (Mg/ha) (Colgan et al., 2013; Naidoo et al., 2015). Plot-level estimates of AGBD are rare and therefore valuable as they form the reference data for the calibration and validation of remote sensing products (Duncanson et al., 2021).

Given the limited spatial coverage and data availability of field AGB data, remote sensing and specifically LiDAR (Light Detection and Ranging) has emerged as a valuable tool for measuring three-dimensional (3D) woody vegetation structures (Lefsky et al., 2002; Lu et al., 2016). LiDAR sensors on a variety of acquisition platforms (ground-based, airborne, spaceborne) collect accurate AGBD-related vegetation measurements, e.g. tree height, Canopy Cover (CC), foliage plant index, at varying spatial scales (Bergen et al., 2009; Camarretta et al., 2019; Coops et al., 2021; Dubayah and Drake, 2000). Plot-level vegetation structural metrics, such as Mean Canopy Height (MCH) and CC, can be derived from discrete return ALS point clouds to develop models that predict AGBD at plot scale (e.g. 25 m^2) (Asner and Mascaro, 2014; Colgan et al., 2012, 2013; Coops et al., 2021; Drake et al., 2002; Lefsky et al., 2002). Compared to optical and radar remote sensing sensors, ALS exhibits significantly fewer signal saturation issues and has the capability to sense properties within the forest canopy, making it a reliable remote sensing technology for predicting AGBD in various forest types (Asner and Mascaro, 2014; Bergen et al., 2009; Ni-Meister, 2015).

Despite the ALS's indisputable advantages, it is expensive resulting in limited spatial and temporal coverages (Atmani et al., 2022; Sothe et al., 2022; Xu et al., 2023), that pose significant challenges to estimating AGBD across larger regions. ALS-based AGBD maps are therefore often used as an intermediary step to scale-up field plot data to spaceborne Synthetic Aperture Radar (SAR) data (Bouvet et al., 2018; Naidoo et al., 2015, 2016; Wessels et al., 2023), or more recently, large-footprint spaceborne LiDAR datasets (Dubayah et al., 2020a; Duncanson et al., 2021; Patterson et al., 2019; Saarela et al., 2022). Spaceborne LiDAR sensors, such as Ice, Cloud and land Elevation Satellite (ICESat-2) and Global Ecosystem Dynamic Investigation (GEDI), have the potential to address this observation gap by providing global and frequent 3D vegetation structural measurements (e.g. vegetation height metrics), which can be used for AGBD estimates in any part of the world. The GEDI instrument is a geodetic-class laser altimeter and large-footprint full-waveform LiDAR designed with a 25 m circular footprint. Launched to the International Space Station (ISS) in 2018, GEDI was the first-of-its-kind laser instrument primarily designed for collecting near-global 3D vegetation structural measurements across Earth's temperate and tropical forests (Dubayah et al., 2020a). GEDI has sampled 4% of Earth's land surface during its four-year mission, providing billions of 3D observations of forest canopy height, vertical profiles, ground elevation, as well as footprint-level AGBD estimates (Dubayah et al., 2020a).

The GEDI's footprint-level (~25 m) AGBD (GEDI L4A) product ($AGBD_{L4A}$) estimates AGBD within individual GEDI footprints. The algorithm used GEDI L2A Relative Height (RH) metrics simulated from reference ALS data along with field data contained in the GEDI Forest Structure and Biomass Database (FSBD) and 13 linear regression models to predict AGBD for individual plant functional type (PFT) within specific geographic regions of the world (Kellner et al., 2023). Even though GEDI L4A models were implemented using the most geographically comprehensive field and LiDAR datasets available in FSBD, some regions, e.g. southern Africa, are still underrepresented (Kellner et al., 2023). In regions with very limited training data, a broad PFT-wide model was applied and in southern Africa a Global Grasses, Shrubs, and Woodlands (GSW) model was used to estimate AGBD (Duncanson et al., 2022; Kellner et al., 2023). It is therefore essential to validate and potentially improve the footprint-level GEDI AGBD estimates for southern Africa, as these are in turn used as geographically expansive reference data to calibrate and validate gridded AGBD maps derived from SAR and optical remote sensing data (Liang et al., 2023; Padalia et al., 2023; Pascual et al., 2023; Silva et al., 2021). Improving GEDI footprint-level AGBD estimates furthermore leads to an improvement in the GEDI L4B AGBD gridded product, which uses hybrid inference to aggregate L4A estimates (25 m) into 1-km cells (Patterson et al., 2019).

Duncanson et al. (2022) anticipated that the L4A footprint-level GEDI AGBD estimates could be locally improved through the incorporation of additional GEDI structural metrics as predictors and supplemental local training datasets, specifically field AGB measurements and ALS data. Recently, a few studies have implemented locally calibrated footprint-level GEDI AGBD models using multiple GEDI metrics (e.g. RH's, Plant Area Index (PAI), Foliage Height Diversity (FHD), Canopy Cover (CC_{GEDI}), etc.) along with ALS and field reference data, with promising results across a wide range of forest types (Bullock et al., 2023; Dorado-Roda et al., 2021; Pascual et al., 2023; Sun et al., 2022; Xu et al., 2023) (see Discussion for details). These studies suggest that footprint-level GEDI AGBD estimates can indeed be improved using local reference datasets and bespoke modeling strategies. However, these studies mostly focused on forests with moderate to high AGBD. Therefore, given the relative scarcity of field AGB and coincident ALS data, no validation of GEDI L4A or local footprint-level AGBD modeling had been conducted in low biomass African savannas, at the time of writing. In our study, we attempted to develop more accurate footprint level AGBD models using ALS based estimates of AGBD as reference data. ALS data were furthermore used to correct for geolocation uncertainty in GEDI data (Li et al., 2023) and thus enabled AGBD models to be calibrated directly with recorded GEDI waveforms rather than simulated waveforms (Duncanson et al., 2022). This approach could expand the range of training data to be more representative of the study domain and conditions the prediction models will subsequently be applied to.

The objectives of this study were to (i) validate GEDI L4A AGBD in South African savannas using field measurements and ALS datasets and (ii) develop and evaluate local GEDI footprint-level AGBD estimates from multiple L2A and L2B metrics. This was accomplished by (1) developing local ALS-based AGBD models using reference field measurements, (2) developing GEDI footprint level AGBD models (Generalized Linear Model - GLM and Random Forest - RF) using multiple selected on-orbit GEDI L2A and L2B metrics as predictors and the ALS AGBD as reference data, and (3) accessing the uncertainty of GEDI L4A and local GEDI AGBD model predictions by comparing them to the reference ALS-based AGBD estimates.

2. Materials and methods

2.1. Study area

Nine study sites were distributed across northern South Africa and representing various savanna vegetation types that fall within Tropical Dry Forests (FAO, 2012) (Fig. 1). Sites were selected to capture a wide diversity of savanna vegetation types, AGBD's and precipitation gradients (mean annual rainfall = 350–723 mm). Land use comprised commercial cattle ranches, communal rangelands, private game reserves, and provincial and national parks. Ireagh, Justicia, Agincourt and Welverdiendt sites are located in the Lowveld of Mpumalanga Province, next to Kruger National Park and include Granite Lowveld and Legogote Sour Bushveld vegetation, as well as small areas of subsistence cultivation containing some large individual trees (Dayaram et al., 2019). The D'Nyala site is situated within the D'Nyala Nature Reserve and contains several Bushveld vegetation types (Table 1), with scattered large Nyala (*Xanthocercis zambesiaca)* and Baobab (*Adansonia digitata*) trees up to 20 m in height. The Venetia site is located at the northern tip of South Africa, in the Musina Mopane Bushveld that is dominated by mopane trees (*Colophospermum mopane*). The three Limpopo sites are primarily dominated by Mopane trees of the Tsende Mopaneveld and Granite Lowveld vegetation types with sporadic pockets of Gravelotte Bushveld and Tzaneen Sour Bushveld (Dayaram et al., 2019). All nine sites mentioned above have predominantly deciduous vegetation that lose their leaves during the dry winters (May to August) (Archibald and Scholes, 2007). The topography of all the sites is flat or gently undulating (mean slope <5.1°) and slope data derived from ALS DEM did not vary much within study sites (standard deviation (STD) < 4°) (Table 1).

2.2. Overview of AGBD modeling

The overall workflow of AGBD modeling was illustrated in Fig. 2 and summarized below.

Step 1: 1 ha and 25 m plot level AGBD calculation

Field measurements (Height and DBH) of individual trees were used to calculated their biomass with an allometric model (**Equation (1)**) (Colgan et al., 2013) and aggregated within each 25 m field plot using **Equation (2)** (Naidoo et al., 2015).

Step 2: Estimating AGBD using ALS data at 25m plot level

Three metrics were extracted from the 1m CHM over the 25m and 1ha field plots: individual tree crown area, MCH, CC. The ALS metrics were used as predictors to produce 25 m and 1 ha ALS-based AGBD estimates using three different methods (**Equations (4)–(6)**). The 25 m $AGBD_{ALS\_area\_MCH\_CC}$ model was subsequently applied within each 25m GEDI footprint to estimate AGBD based on ALS CHM.

Step 3: Validation of footprint-level $AGBD_{L4A}$ estimates

All GEDI footprints coinciding with the ALS data were selected after quality filtering and excluding leaf-off periods (Li et al., 2023) (Fig. 3). The collocateWaves program in gediSimulator was used to remove the systematic component of geolocation uncertainty (1 sigma = 10 m) GEDI footprint data products (Hancock et al., 2019).

Step 4: Estimating local GEDI AGBD using on-orbit GEDI metrics

Finally, random forest (RF) and generalized linear models (GLM) were developed with footprint-level ALS-based AGBD as the response variable and the on-orbit GEDI L2A and L2B datasets as predictor variables.

2.3. Data

2.3.1. Field data

Field data were collected in 2017 and 2018 between April–May and November–December across 20 sampling plots in Justicia, D'Nyala, Venetia, and Welverdiendt (Fig. 4). Ground sampling plots were chosen based on their representativity of the diversity in woody vegetation structure, vegetation type, approximate CC range, management regimes and geological substrates across the savanna study sites. The 100 m × 100 m plots were positioned using high-resolution imagery from Google Earth to ensure that they were representative according to the aforementioned landscape characteristics and that they were accessible. Field AGB estimates of individual trees were derived from height and stem diameter measurements using the following allometric AGB estimation model (Colgan et al., 2013):

$$M = 0.109 \times D^{(1.39+0.14\times \ln(D))} \times H^{0.73} \times \rho^{0.8} \quad (1)$$

where M = aboveground biomass in kg, D = Diameter at Breast Height

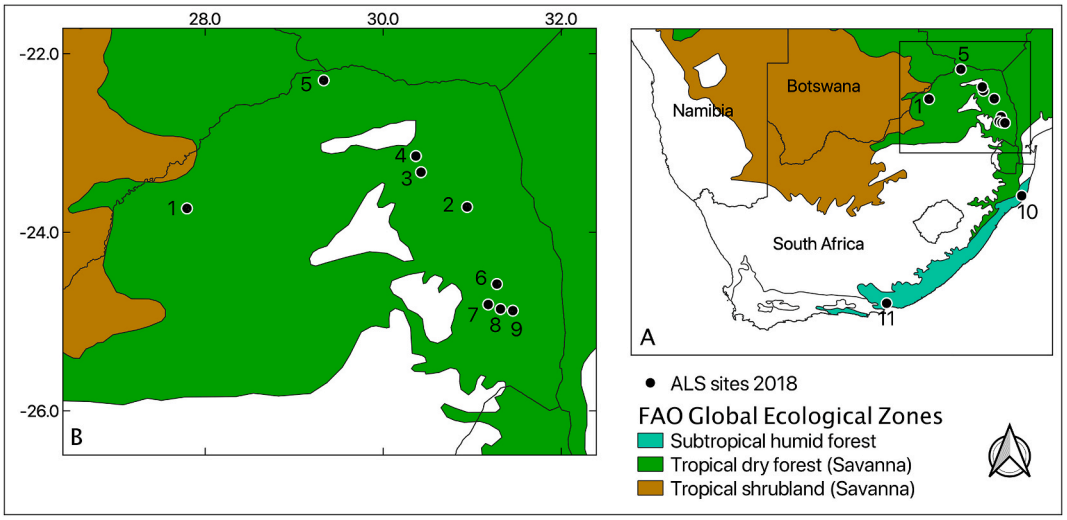

Fig. 1. (A) Study area within South Africa with relevant FAO Global Ecological Zones. (B) Inset of northern South Africa with detailed location of individual sites covered by airborne LiDAR data (ALS): (1) D'Nyala, (2, 3, 4) Limpopo, (5) Venetia, (6) Welverdiendt, (7) Agincourt, (8) Ireagh, (9) Justicia. Four sites (1, 5, 6, 9) contained field plots where plot-level AGBD was estimated.

Table 1
Properties of study sites and airborne LiDAR (ALS) metrics.

Site#	Site name	Vegetation type (Dayaram et al., 2019)/transformed cover	Mean annual rainfall (mm)	Mean (STD) ALS height (m)	ALS canopy cover (%)	Date of ALS	Area (km^2)	Mean (STD) Slope (°)
1	D'Nyala	Roodeberg, Waterberg Mountain & Limpopo Sweet Bushveld	375	3.9 (2.3)	74.3	March 2018	53.26	2.36 (3.69)
2.3.4	Limpopo	Tsende Mopaneveld, Granite Lowveld, Gravelotte Bushveld & Tzaneen Sour Bushveld	613	3.3 (2.1)	51.5	March/ April 2018	163.32	1.7 (1.28)
5	Venetia	Musina Mopane Bushveld & Limpopo Ridge Bushveld	368	2.5 (1.1)	41.6	March 2018	56.31	1.97 (1.75)
6	Welverdiendt	Granite lowveld & Legogote Sour Bushveld/subsistence cultivation	353	3.7 (2.0)	44.2	June 2018	126.75	1.74 (1.68)
7	Agincourt	Granite lowveld & Legogote Sour Bushveld/subsistence cultivation	353	4.2 (2.4)	41.9	May 2018	35.88	5.14 (4.84)
8	Ireagh	Granite lowveld & Legogote Sour Bushveld/subsistence cultivation	687	3.2 (2.3)	32.3	June 2018	65.08	2.43 (2.09)
9	Justicia	Granite lowveld & Legogote Sour Bushveld/subsistence cultivation	550	3.4 (2.5)	28.9	June 2018	81.25	2.55 (1.48)

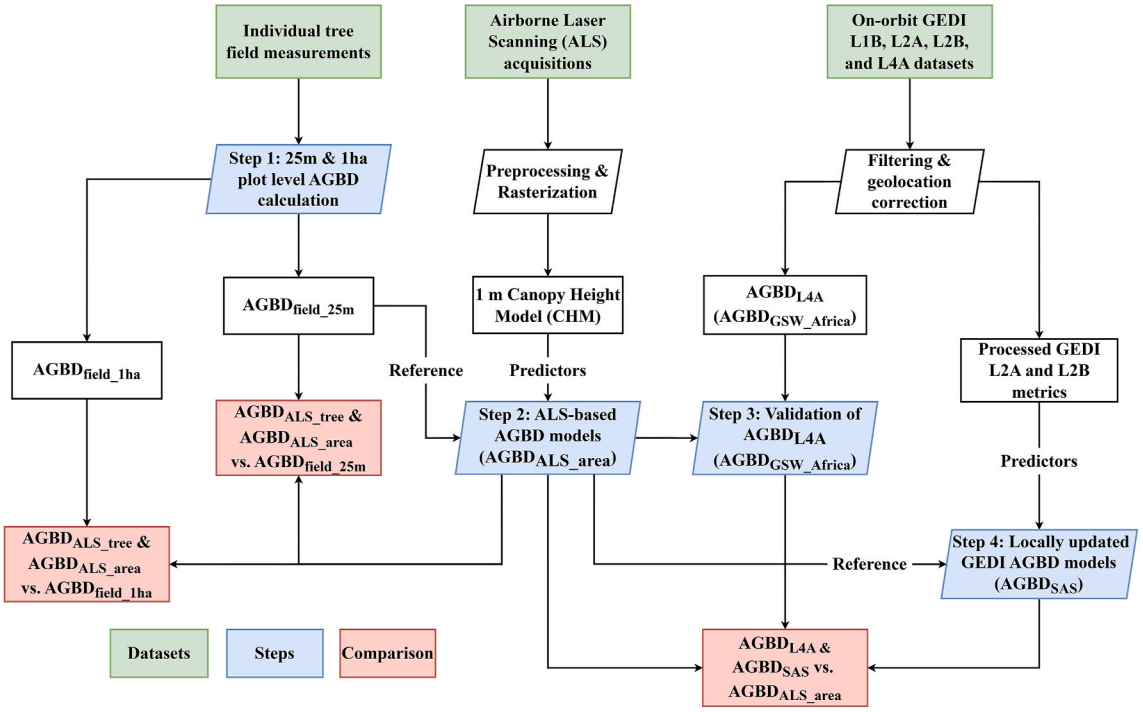

Fig. 2. Workflow of field measurement, ALS, and GEDI data processing and analysis.

Fig. 3. Cross-section of normalized ALS point cloud data showing GEDI 25m footprints and corresponding GEDI Relative Height 98 (RH98) and GEDI L4A aboveground biomass density (AGBD).

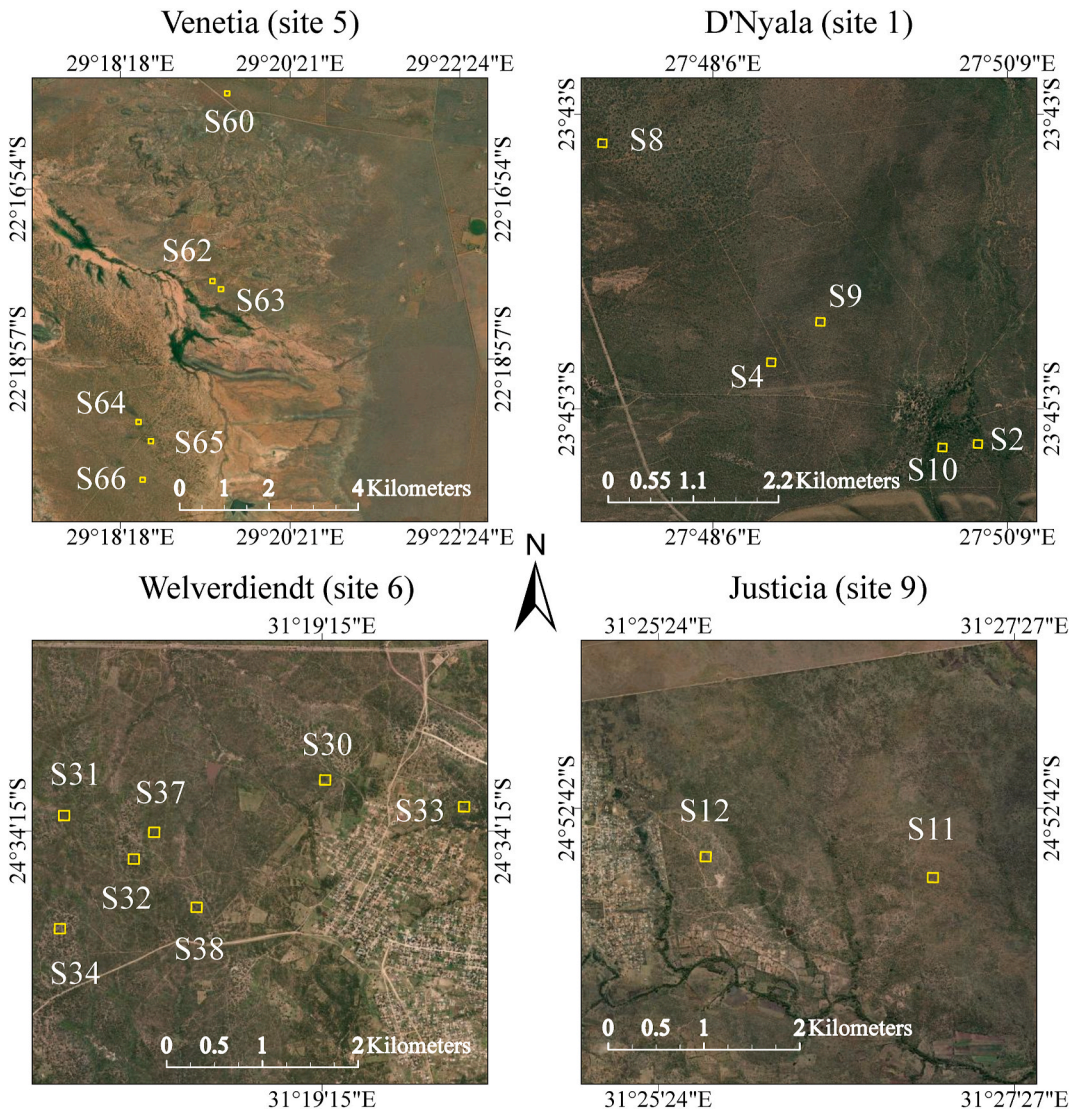

Fig. 4. 1 ha field plots within sites: Venetia (site 5, S60, S62-66), D'Nyala (site 1, S2, S4, S8-10), Welverdiendt (site 6, S30–34, S37-38), and Justicia (site 9, S11-12). Location of sites were given in Fig. 1. (Image: Google, © 2020 Maxar Technologies).

(DBH) in cm, H = height of tree in m, and ρ = mean wood specific gravity (unitless and fixed at a mean value of 0.8).

The allometric model was developed following the destructive harvesting of 17 savanna tree species present in the study area (N = 707; R^2 = 0.98; relative Root Square Error = 52%; ranging from 0.2 to 4531 kg per tree, (Colgan et al., 2013). Tree height was measured using a height pole for shorter trees (<7 m) and Laser vertex/rangefinder for taller trees (>7 m), while stem diameter was measured using calipers and diameter at breast height (DBH) tape. Stem diameter was measured at 10 cm above the ground and individual stems of multi-stemmed plants were measured as separate individuals (e.g. species such as *Dichrostachys cinerea,* as well as trees which have coppiced due to fuelwood harvesting).

Three main stem diameter 'zones' were identified inside the plot to increase AGB sampling efficiency, whilst yielding representative measurements within the 1 ha sized sample plot (modified from Naidoo et al. (2015)) (Fig. 5). The purpose of this sampling design was to ensure that AGBD estimates could be derived at both the 25 m × 25 m and at the 100 m × 100 m scale for ALS AGBD model prediction and for GEDI-derived AGBD estimation. DBH Zone 1 was the 10 m × 10 m plots positioned on the inner corner of the four corner 25 m × 25 m plots where all trees with a stem diameter ≥3 cm were measured. The DBH Zone 2 was the 25 m × 25 m plot, located at each of the four corners of the 1 ha sample plot, where all trees with a stem diameter ≥5 cm were measured. DBH Zone 3 was the remaining 25m plots within the 1 ha plot, where all trees with a DBH ≥10 cm were measured (Fig. 5). This sampling design allows the efficient measurement of multi-stemmed, coppicing plants with low DBH that contributes little AGB (Matsika et al., 2013). A total of 203 valid 25 m × 25 m field plots and 20 valid 100 m × 100 m field plots were sampled (Fig. 6).

After individual tree level AGBD was derived using equation (1) (Colgan et al., 2013), 25 m field plot AGBD ($AGBD_{field\_25m}$) was calculated for each 25 m diameter zone by summing the relevant tree level AGB values multiplied by a scaling factor (equation (2)):

$$AGBD_{field\_25m} = Q + S + 6.25 \times T \quad (2)$$

where 'Q' is the total AGB of stems ≥ 10 cm DBH, 'S' is total AGB of stems between 5 and 10 cm DBH and 'T' is the total AGB of stems between 3 and 5 cm DBH. The scaling factor of 6.25 was used as stems between 3 and 5 cm were only sampled within the 10 by 10 m (i.e., DBH zone 1; 16% of 25 m plot) subplot and not sampled for the rest of the 25 m × 25 m grid (i.e., DBH zone 2). This scaling factor assumes the 10 m × 10 m subplot measurements are a representative sample of the 3–5 cm size class for all 25 m subplots in the 1 ha plot.

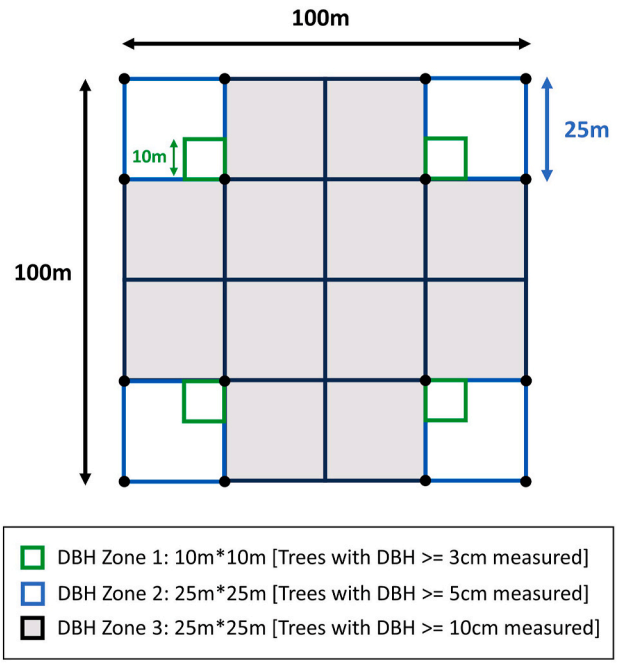

Fig. 5. Ground sampling design for generating estimates of woody AGBD (Naidoo et al., 2015).

The 1 ha plot level AGBD ($AGBD_{field\_1ha}$) was calculated by summing all the tree-level AGB within each diameter zone and multiplied by specific AGBD scaling factors (equation (3)) to account for the trees not measured within the sub-sample plots. The sample plot AGBD values (at both the 25 m and 1 ha) were converted to the units of megagrams per hectare (Mg/ha).

$$AGBD_{field\_1ha} = A + 4 \times B + 25 \times C \quad (3)$$

Where 'A' is the total AGB of stems greater than 10 cm DBH (i.e. DBH zone 3; 100% of plot), B is the total AGB of stems between 5 and 10 cm DBH (within the DBH zone 2; 25% of plot) and C is the total AGB of stems between 3 and 5 cm DBH (within the DBH zone 1; 4% of plot). The scaling factors of 4 and 25 were used for DBH zones 2 and 1, respectively.

2.3.2. Airborne laser scanning (ALS) data

Approximately 550 km^2 of discrete ALS data were collected between March and June of 2018 (Table 1) over the nine study sites (Fig. 1). The airborne LiDAR datasets were collected from a fixed wing aircraft (700 m above ground) using Optech ALTM M300 (13SEN327) and Optech Gemini (09SEN258) sensors at a pulse repetition rate of 150 kHz. Acquisitions were planned to have 25% overlap between flight lines and resulted in an average laser spot spacing of 0.4 m and an average point density of 8.6 points/m^2. Digital terrain models (DTM), digital surface models (DSM), and canopy height models (CHM) were generated from the ALS data at 1 m resolution, using *lidR* package (Roussel et al., 2018) in R. The Grid_canopy (lidR package) function was used to generate CHMs at 1 m resolution using DSM Algorithm (p2r) without any smoothing or filtering. Within each 25 m field plot (Fig. 6), the LiDAR CC variable was calculated by dividing the number of the 1 m CHM pixels with heights above 0.5 m by the total number of CHM pixels. The MCH was also calculated by averaging CHM pixels above a height threshold of 0.5 m to avoid potential grass and coarse woody debris components (Naidoo et al., 2015).

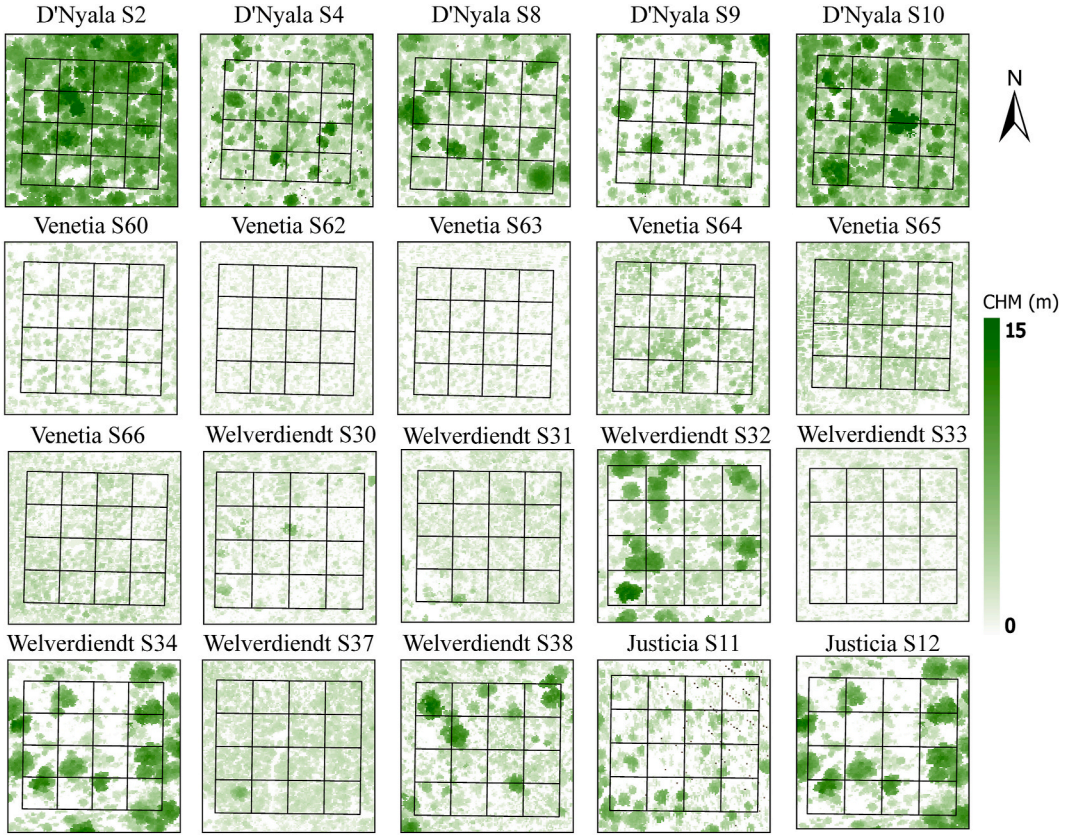

Fig. 6. 25 m plots within the 1 ha field plots displayed over 1m ALS canopy height model. For the location of sites and plots see Fig. 1 and 2. (D'Nyala, Venetia, Justicia, and Welverdiendt).

2.3.3. GEDI data

GEDI was specifically designed to measure vegetation structure and estimate AGBD (Dubayah et al., 2020a) over Earth's tropical and temperate forests. The multi-beam LiDAR provides eight tracks (four full-power beam tracks and four coverage beam tracks) of GEDI footprints, with a nominal diameter of 25 m and 60 m along track spacing and 600 m across track spacing. The study used all Version 2 L1B, L2A, L2B, and L4A GEDI data products (Dubayah et al., 2020b, 2021a, 2021b, 2021c) coincident with the ALS extent of study sites up until August 2022 and available from NASA's Earth Science Data Systems (ESDS). GEDI data have a known systematic geolocation uncertainty of approximately 10m (1 standard deviation) (Beck et al., 2021) that can be reduced by through maximizing the correlation between on-orbit GEDI waveforms and simulated GEDI waveforms using gediSimulator's collocateWaves function (Hancock et al., 2019; Hofton et al., 2000; Li et al., 2023). This process reduced geolocation error between the GEDI on-orbit and ALS-simulated waveforms, however some local time dependent geolocation error may remain in the on-orbit GEDI waveform positions (Schleich et al., 2023). Geolocation error of 0–2 m caused by random jitter on the GEDI instrument remains in the corrected GEDI footprint locations, which contributes 14–20% of overall error in RH98 estimation when compared to ALS-simulated GEDI waveforms (Li et al., 2023).

In this study, 40 GEDI orbits intersected nine study sites, providing a total of 9855 useful GEDI footprints (samples) between April 2019 and August 2022, which was all the data released at the time of writing. Several metrics were extracted from GEDI data products for AGBD modeling, including GEDI L2A, L2B, and L4A quality flags, sensitivity, GEDI L2A relative heights (RHs), GEDI L2B PAI, FHD, CC, and GEDI L4A AGBD estimates ($AGBD_{L4A}$). The definitions and descriptions of these metrics were listed in Table 2.

The L4A product includes estimates of footprint-level AGBD that were produced using Ordinary Least Squares (OLS) regressions predicting AGBD as a function of simulated L2A RH metrics. These were simulated using a global database of field plot AGBD (estimated using generalized allometries) and discrete-return airborne LiDAR that were used to simulate RH metrics (Hancock et al., 2019). This database was divided by Plant Functional Type (PFT) and continental region, with one of 13 linear models assigned to each of these regions (Duncanson et al., 2022). In South Africa, the L4A product currently uses a global GSW model to predict AGBD using only the RH98 metric (Duncanson et al., 2022; Kellner et al., 2023).

Quality flags were used to remove low-quality waveforms. Only land surface GEDI footprints with all GEDI L2 and GEDI L4 quality flags = 1 were considered as "good quality" data when specific requirements were met in terms of waveform fidelity and beam sensitivity (>0.95). It was previously demonstrated that the phenological conditions of vegetation at the time of GEDI data acquisition had a very large influence on GEDI canopy height metrics (RH98) in deciduous savannas, with RH98 being underestimated by 1.47 m and a %RMSE of 41% (Li et al., 2023). During leaf-off conditions, the GEDI LiDAR signal may have lower amplitude returns at the canopy top as it interacts with denuded branches, resulting in lower detected canopy top and therefore a large negative height bias in the derived RH98 measurements. Given that RH98 is an important predictor variable of AGBD, GEDI footprints with leaf-off and transitional phenological conditions between May and October were excluded to ensure the most accurate AGBD estimates.

Table 2
The definitions of GEDI metrics (Hofton and Blair, 2020; Kellner et al., 2023; Tang and Armston, 2019).

GEDI Metric	Description
Sensitivity (unitless)	Maximum canopy cover that can be penetrated considering the SNR of the waveform
FHD (unitless)	Foliage height diversity (FHD) index calculated by vertical foliage profile normalized by total plant area index (PAI).
Cover (%)	GEDI canopy cover. The percentage of the ground covered by the vertical projection of canopy material.
PAI (m^2 m^{-2})	GEDI Plant Area Index (PAI). One half of the total plant area per unit ground surface.
RH metrics (m)	GEDI RH metrics, including RH50, RH75, RH90, and RH98.
$AGBD_{L4A}$ (Mg/ha)	The GEDI's footprint-level (~25 m) AGBD (GEDI L4A) product

2.4. AGBD modeling

2.4.1. ALS-based AGBD prediction

A total of 6731 individual trees were measured in the field. Since it is unlikely that a GEDI footprint will coincide with a field plot, ALS data were first used to estimate AGBD across the entire extent of the ALS data, which coincided with many GEDI footprints that could then be used for modeling. Typically, this processing involves matching ALS to the spatial extent of field plots, developing empirical AGBD models to estimate field plot level AGBD from ALS, and the application of the developed AGBD model to ALS data within all GEDI footprints. Several studies that focused on the validation and calibration of tree-based methods and area-based AGBD modeling have been conducted within some of these study sites or in neighboring Kruger National Park (Colgan et al., 2012, 2013; Naidoo et al., 2015). In this study, three models were implemented and evaluated to estimate AGBD based on locally estimated ALS derived metrics and field plot measurements.

(1) Tree-based AGBD model: Colgan's tree-based AGBD ($AGBD_{ALS\_tree}$) (Colgan et al., 2013) was developed using harvested trees with more than 3000 stems, weighing ~57,000 kg in Phalaborwa and Kruger National Park, South Africa. The modeling process consists of four parts: (i) segmentation of ALS-derived CHMs into tree crown objects (Dalponte and Coomes, 2016), (ii) extraction of maximum canopy height (m) and tree crown area (m^2) for each crown object, (iii) prediction of AGB (kg) for each crown object (Colgan et al., 2013), and (iv) summation of crown-level AGBD within each 25 m field plot to estimate plot-level $AGBD_{ALS\_tree}$ (Mg/ha). The resulting tree-based model was shown as follows:

$$m = 10^{0.0207+0.3\times\left(log\ 10(CA)+0.196*(log\ 10(CA))^2+1.74\times(log\ 10(H))\right)} \quad (4)$$

where "m" is the aboveground biomass of the tree (kg); "CA" is the crown area (m^2) derived from segmentation process, and "H" represents the maximum heights (m) of CHM within individual tree crowns.

(2) Area-based, height AGBD power model ($AGBD_{ALS\_area\_MCH}$): this model uses ALS MCH and was evaluated in this study area by Colgan et al. (2012) who used a linear function for relationship between MCH and AGBD. In the current study we used a power function (Asner et al., 2012; Asner and Mascaro, 2014; Meyer et al., 2013):

$$AGBD_{ALS\_area\_MCH} = a \times MCH^b \quad (5)$$

where "AGBD" is aboveground biomass density (Mg/ha) and "MCH" is the mean canopy heights (m) within each field plot.

(3) Area-based, height and cover AGBD linear model ($AGBD_{ALS\_area\_MCH\_CC}$): this model uses ALS derived CC and mean canopy heights (MCH) (Colgan et al., 2012, 2013) in linear model relating AGBD to the product of MCH and CC. Colgan et al. (2012) identified MCH × CC as the most reliable predictor variable and the model was extensively used in the study area (Davies et al., 2018; Davies and Asner, 2019; Naidoo et al., 2015). The model was adjusted to pass through the origin (0, 0) without including an intercept term, while also accounting for minimum AGBD values set to 0.

$$AGBD_{ALS\_area\_MCH\_CC} = a \times MCH \times CC \quad (6)$$

where "AGBD" is aboveground biomass (Mg/ha), "CC" is canopy cover and "MCH" is the mean canopy heights (m) within each field plot. The $AGBD_{ALS\_area\_MCH\_CC}$ model was subsequently applied within each 25m

GEDI footprint to estimate AGBD based on ALS CHM.

2.4.2. GEDI L4A AGBD estimates

It was previously established that the best performing models for estimating GEDI footprint-level AGBD ($AGBD_{L4A}$) were developed from an exhaustive set of candidate GEDI RH predictors for different plant functional types (PFT) and geographic regions (Duncanson et al., 2022). The model selection frequently preferred combinations of a few simulated GEDI RH metrics, such as RH98, RH90, RH50, and RH10. However, GEDI RH98 was selected as the single predictor to develop Grasses, Shrubs, and Woodlands (GSW) model which was applied to the southern African savannas (Kellner et al., 2023). Given than only one type of L4A model was implemented in Southern Africa, $AGBD_{L4A}$ is equivalent to the GSW Africa AGBD ($AGBD_{GSW\_Africa}$) which was calculated using the following equation:

$$AGBD_{L4A} = 1.118 \times \left(-124.832 + 12.426 \times \sqrt{RH98 + 100} \right)^2 \quad (7)$$

Where "$AGBD_{L4A}$" is the GEDI L4A AGBD (GSW model applied only), "RH98" is on-orbit GEDI RH98 metrics.

2.4.3. Development of local GEDI AGBD prediction models

The 25 m $AGBD_{ALS\_area\_MCH\_CC}$ model was used to predict AGBD within each 25m GEDI footprint (n = 7125) based on the ALS CHM. This was used as the reference data for the development of local footprint level GEDI AGBD models using (i) a generalized linear model (GLM) and (ii) random forest (RF).

2.4.3.1. Generalized linear model (GLM). GLM's were developed to explicitly account for heteroscedasticity and the non-normal error distribution of the response variable (AGBD). Following the GLM model specification presented in Fatoyinbo et al. (2021), a Gamma distribution was selected to model the continuous, non-negative, and positively skewed AGBD data. Multiple on-orbit GEDI L2A and L2B metrics GEDI canopy cover (CC_{GEDI}), and FHD, PAI and RH metrics were assessed for potential inclusion in a local GEDI AGBD model (**Appendix 1**). The Variance Inflation Factor (VIF) of each predictor variable was used to determine any potential correlation of the variable with other metrics. This study considered VIF >10 as an indicator of multicollinearity. We also excluded predictor pairs with a correlation coefficient greater than 0.8, to avoid model multicollinearity and minimize the number of candidate predictor variables. For example, PAI in the current GEDI Level-2B Version 2 product uses global constants for canopy architecture, therefore it may be derived directly from CC_{GEDI} without any prior knowledge. Therefore, neither were included in the final model. Following exhaustive model selection, only GEDI RH50, RH98 and FHD were identified as the predictor variables based on relatively low VIF and correlation coefficient values, combined with the highest R^2 (**Appendix 1**). The GLM using GEDI RH50, RH98 and FHD as predictors was implemented and referred to as the local South African Savannas (SAS) GEDI AGBD using GLM" ($AGBD_{SAS\_GLM}$) (equation (8)).

$$AGBD_{SAS\_GLM} = a \times RH98 + b \times (RH50 + 100) + c \times FHD + d \quad (8)$$

Where "RH98", "RH50", and "FHD" are GEDI RH98, GEDI RH50, and Foliage Height Diversity (FHD), respectively, and "a", "b", "c" and "d" are model constants.

2.4.3.2. Random forest (RF). RF are non-parametric machine learning models that are widely used for predicting biophysical variables, including AGBD, from remote sensing data (Breiman, 2001; Leite et al., 2022; Wessels et al., 2019; Xu et al., 2023; Zhang et al., 2022). RF models were implemented to predict AGBD from GEDI L2A (RH50, RH75, RH90, RH98) and L2B metrics (sensitivity, FHD, and CC_{GEDI}) (n = 7125). PAVD and PAI were not included because of their high correlation with CC_{GEDI}, from which they were derived (Appendix 1). RH100 was not included because it is more sensitive to noise than RH98 (Blair and Hofton, 1999). The remaining metrics were used as predictors in RF models using *train* function in R package *carat* (Ma et al., 2023). After using the grid search for hyperparameter tuning, "number of trees", "mtry", and "node size", "trainControl" were set to 300, 3, 4, and "5-fold cross-validation", respectively. The GEDI AGBD obtained was referred to as "local South African Savannas (SAS) GEDI AGBD using RF" ($AGBD_{SAS\_RF}$).

2.5. Evaluation of GEDI AGBD estimates against ALS AGBD reference data

Using the ALS AGBD as reference values within each GEDI footprint, model accuracy of $AGBD_{SAS\_GLM}$ and $AGBD_{SAS\_RF}$ was assessed using 5-fold cross-validation. Several statistical metrics were used to evaluate model performance, including the coefficient of determination (R^2) and the error measures given in equation (9-13): the systematic difference between GEDI AGBD and reference ALS-based AGBD ($AGBD_{diff}$), the Mean Systematic Deviation (MSD), the Relative Mean Systematic Deviation (RMSD), the Root Mean Square Error (RMSE), and the relative RMSE (%RMSE). Systematic deviation refers to the systematic difference between the predicted AGBD and the reference AGBD and is equivalent to bias when the plot values are unbiased (Duncanson et al., 2021). Given that our field plot AGBD values may be biased, we therefore opted for RMSD.

$$AGBD_{diff} = AGBD_{GEDI} - AGBD_{ALS} \quad (9)$$

$$MSD = \frac{\sum_{i=1}^{n} (AGBD_{diff})}{n} = \frac{\sum_{i=1}^{n} Bias_i}{n} \quad (10)$$

$$RMSD = \frac{MSD}{mean(AGBD_{ALS})} \times 100 \quad (11)$$

$$RMSE = \sqrt{\frac{\left(\sum_{i=1}^{n} AGBD_{diff}\right)^2}{n}} \quad (12)$$

$$\%RMSE = \frac{RMSE}{mean(AGBD_{ALS})} \times 100 \quad (13)$$

Where $AGBD_{GEDI}$ and $AGBD_{ALS}$ are GEDI and ALS estimated AGBD, respectively.

3. Results

3.1. Development of ALS-based AGBD models

3.1.1. AGBD estimation using ALS data at 1 ha plot level

The AGBD of the field data ranged from 2.04 Mg/ha to 159.4 Mg/ha, with a mean of 28.8 Mg/ha. AGBD was accurately estimated at 1 ha plot level by both tree-based and area-based AGBD models when compared to the field measurements, with R^2 values greater than 0.82 (Fig. 7). The tree-based method significantly underestimated AGBD, with an MSD of −7.2 Mg/ha (Fig. 7 a), which was much larger than that of the area-based MSD of 0–1 Mg/ha (Fig. 7 b, c).

3.1.2. AGBD estimation using ALS data at 25 m plot level

The average AGBD of all 25 m field plots was 21.5 Mg/ha (STD = 28.2 Mg/ha), with the maximum AGBD of 165.5 Mg/ha in D'Nyala S2 site. The 25 m $AGBD_{ALS\_area\_MCH}$ predictions were more accurate than 25 m $AGBD_{ALS\_tree}$ predictions, with a much higher R^2 (0.77 vs. 0.64) and lower RMSE (14.0 vs. 20.6 Mg/ha) (Fig. 8 a, b). The area-based AGBD model using MCH × CC ($AGBD_{ALS\_area\_MCH\_CC}$) was also better than the 25 m $AGBD_{ALS\_tree}$ model, with an R^2 of 0.7 and RMSE of 15.7 Mg/ha (Fig. 8 c). Although the power function (MCH) and linear MCH × CC models had similar error metrics, the distribution of their AGBD

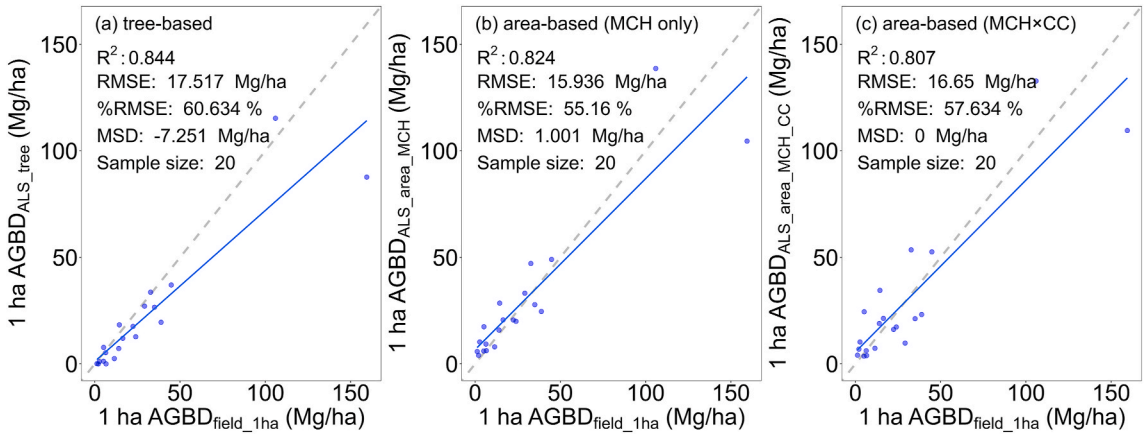

Fig. 7. Scatterplots of ALS-based AGBD vs. AGBD field measurements at 1 ha level. a: tree-based method; b: area-based method (MCH only); c: area-based method (MCH × CC).

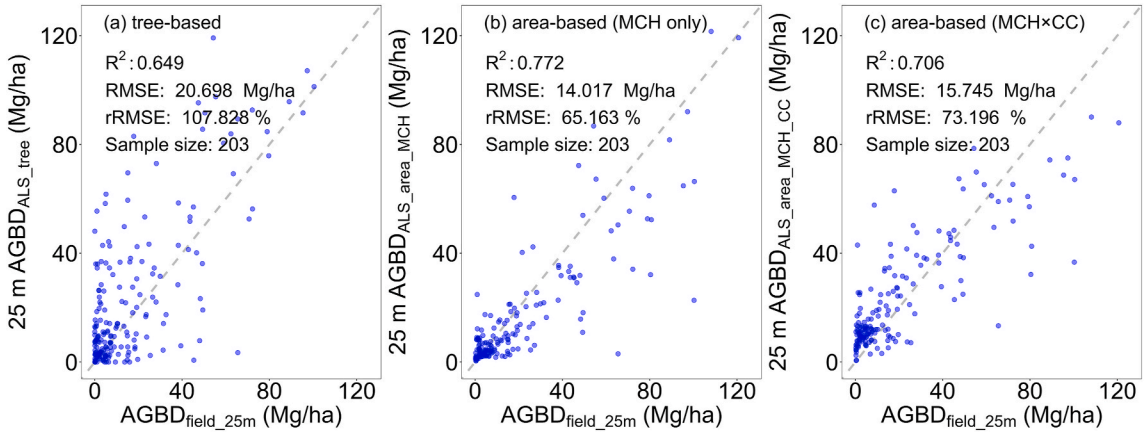

Fig. 8. Scatterplots of ALS-based AGBD vs. AGBD field measurements at 25 m level. a: tree-based method; b: area-based method (MCH); c: area-based method (MCH × CC).

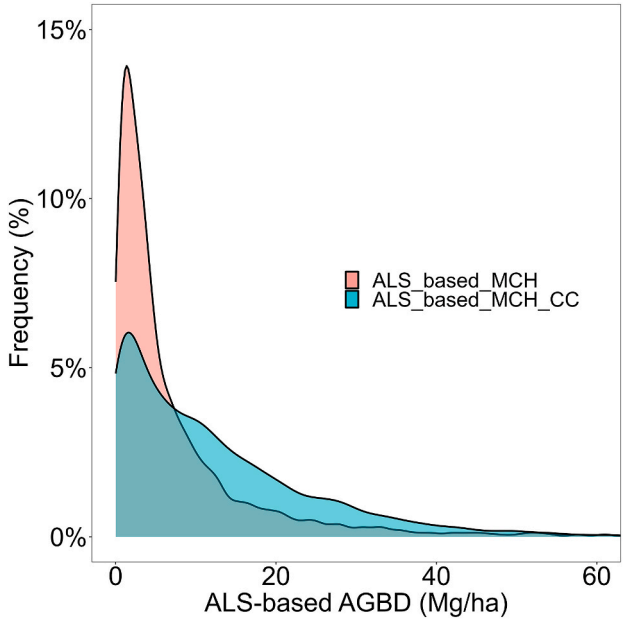

Fig. 9. Smoothed density plot of the relative frequency of 25 m ALS-based AGBD estimated by two models: $AGBD_{ALS\_area\_MCH}$ (red) and $AGBD_{ALS\_area\_MCH\_CC}$ (blue).

predictions were very different (Fig. 9). The 25 m $AGBD_{ALS\_area\_MCH}$ consequently overestimated the abundance of areas in the 0–5 Mg/ha bin while significantly underestimating areas in the 10–35 Mg/ha range. The 25 m $AGBD_{ALS\_area\_MCH\_CC}$ had AGBD predictions that were double that of 25 m $AGBD_{ALS\_area\_MCH}$ (Mean AGBD: 12 Mg/ha vs. 7.4 Mg/ha). When comparing the MSD distribution, 25 m $AGBD_{ALS\_area\_MCH}$ consistently underestimated slightly, up to 30 Mg/ha, above which it significantly underestimated, by 7–17 Mg/ha (Fig. 10). In contrast, 25 m $AGBD_{ALS\_area\_MCH\_CC}$ overestimated slightly by about 5 Mg/ha up to 30

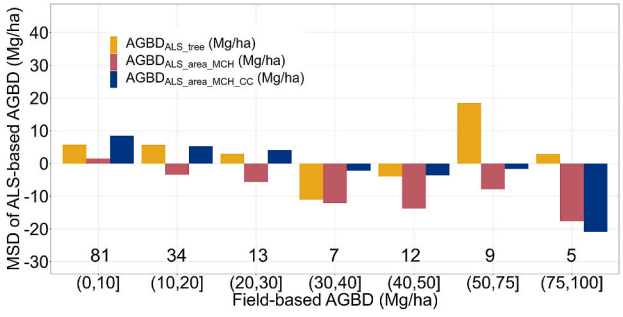

Fig. 10. Histogram of Mean Systematic Deviation of yellow: $AGBD_{ALS\_tree}$; red: $AGBD_{ALS\_area\_MCH}$; blue: $AGBD_{ALS\_area\_MCH\_CC}$ vs. field estimated $AGBD_{field\_25m}$. $AGBD_{field\_25m}$ values were binned at 10 Mg/ha increments up to 50 Mg/ha, and in increments of 25 Mg/ha from 50 Mg/ha to 100 Mg/ha. The bottom row of numbers represents bin counts.

Mg/ha, however, the MSDs were very low (MSD <5 Mg/ha) and did not increase in the midrange bins of 10–50 Mg/ha. $AGBD_{ALS\_area\_MCH\_CC}$ had a very modest underestimation of MSD <5 Mg/ha between 20 and 75 Mg/ha. The rest of the modeling (step 3–4) and results were based on the area-based method using MCH × CC (Fig. 8 c).

3.2. Validation of GEDI L4A and local GEDI AGBD estimates

There was a moderate to strong positive relationship between GEDI footprint-level AGBD estimates by the $AGBD_{L4A}$, $AGBD_{SAS\_GLM}$, $AGBD_{SAS\_RF}$ models and 25m reference $AGBD_{ALS\_area\_MCH\_CC}$, with R^2 of 0.42, 0.53, 0.71 respectively (Fig. 11 a, b, c). $AGBD_{L4A}$ underestimated AGBD with an MSD of −3.8 Mg/ha. $AGBD_{SAS\_GLM}$ had an MSD of 1.4 Mg/ha, while $AGBD_{SAS\_RF}$ had an MSD close to 0 Mg/ha. $AGBD_{SAS\_GLM}$ and $AGBD_{SAS\_RF}$ (Fig. 11 b, c) had lower RMSE's of 10.2 Mg/ha (%RMSE = 67.2%) and 7.3 Mg/ha (%RMSE = 53.3%) respectively, compared to $AGBD_{L4A}$ with an RMSE of 12 Mg/ha (%RMSE = 79.5%).

The MSD distribution within specific AGBD bins were investigated across the range of AGBD values. Given the low overall AGBD values in savannas, the absolute MSD remained below 18 Mg/ha across all bins for all three GEDI AGBD models (Fig. 12). $AGBD_{SAS\_GLM}$ and $AGBD_{SAS\_RF}$ overestimated slightly by less than 3–4.4 Mg/ha, below 15 Mg/ha, but they increasingly underestimated in bins above 20 Mg/ha by 11%–22% RMSD. $AGBD_{L4A}$ underestimated the most of all the models, especially in the 15–50 Mg/ha bins with RMSD of −21% to −37.9%, while the local models ($AGBD_{SAS\_GLM}$ and $AGBD_{SAS\_RF}$) underestimated much less (−1.5% to −24.1%) in the bins that make up the bulk of the mid-range estimates (Fig. 12). $AGBD_{SAS\_GLM}$ and $AGBD_{SAS\_RF}$ underestimated with a mean of −3.4 Mg/ha (−8.6%) and −5.5 Mg/ha (−15.2%) respectively for the bins between 15 and 50 Mg/ha, while $AGBD_{L4A}$ exceeded 20% underestimation for almost all bins above 10 Mg/ha. Only 2.8% of data points fell inside the aggregated highest bin of 50–75 Mg/ha where the underestimation stabilized at RMSD of 10% and 23% respectively for GBD_{SAS_GLM} and $AGBD_{SAS\_RF}$. The $AGBD_{SAS\_GLM}$ provided the lowest mean RMSD of 9.2% across the range of bins above 10 Mg/ha, which was consistently about half that of $AGBD_{SAS\_RF}$, especially in the 20–40 Mg/ha range (Fig. 12 b, c).

4. Discussion

GEDI has collected billions of 3D structural observations between April 2019 and March 2023, enabling near-global AGBD estimates (Dubayah et al., 2022). The GEDI mission's calibration and validation of the AGBD estimations have largely focused on temperate and tropical forests to satisfy the GEDI mission Level 1 requirements (Fatoyinbo et al., 2021; Hancock et al., 2019; Qi et al., 2019; Sun et al., 2022). As a result, the use of GEDI data for estimating AGBD in savannas has received limited attention, until recent renewed interest in carbon storage by trees in drylands (Skole et al., 2021; Tucker et al., 2023). To our knowledge, this paper was the first to validate the GEDI $AGBD_{L4A}$ product in African savannas. In addition, local GEDI AGBD models were developed using multiple on-orbit GEDI metrics to improve the accuracy of the footprint-level AGBD estimates.

Both tree-based and area-based approaches for estimating ALS-based AGBD were tested. Multiple previous studies have used individual tree crown segmentation from ALS data to delineate trees (Dalponte and Coomes, 2016; Duncanson et al., 2014; Ferraz et al., 2016b; Holmgren and Persson, 2004; Li et al., 2012; Silva et al., 2016) and calculate tree-based AGBD from the individual tree crown metrics (Colgan et al., 2013; Ferraz et al., 2016a). The area-based methods performed better than the tree-based method, which was consistent with several other studies comparing these two approaches (Coomes et al., 2017; Duncanson et al., 2015; Maltamo et al., 2009). The inferior performance of the tree-based method could be due to the limited detectability of understory trees, as noted by Duncanson et al. (2021) along with the unreliability of the segmentation algorithm used to identify tree crowns in complex savannas. The 25 m $AGBD_{ALS\_area\_MCH\_CC}$ provided the most realistic distribution of predicted AGBD (Fig. 9), similar to those of previous studies in this area (Colgan et al., 2013; Davies et al., 2018; Naidoo et al., 2015). Additionally, the 25 m $AGBD_{ALS\_area\_MCH\_CC}$ also had the lowest MSD values compared to the other two methods across the range of 10–75 Mg/ha (Fig. 10) and therefore, $AGBD_{ALS\_area\_MCH\_CC}$ was used in all the subsequent evaluations of the GEDI footprint-level AGBD.

The L4A product was compared to ALS based AGBD estimates alongside the local models of footprint-level AGBD. The local models, i.e. $AGBD_{SAS\_GLM}$ and $AGBD_{SAS\_RF}$ had a much stronger relationship with the reference 25 m $AGBD_{ALS\_area\_MCH\_CC}$ than L4A ($R^2 = 0.42$) with R^2 of 0.53 and 0.71 respectively (Fig. 11a, b, c). $AGBD_{SAS\_GLM}$ and $AGBD_{SAS\_RF}$ (Fig. 11b, c) had significantly lower RMSE's of 10.2 Mg/ha (%RMSE = 67.2%) and 7.3 Mg/ha (%RMSE = 53.3%) respectively, compared to $AGBD_{L4A}$ (RMSE = 12 Mg/ha, %RMSE = 79.5%). The local $AGBD_{SAS\_RF}$ and $AGBD_{SAS\_GLM}$ models therefore outperformed GEDI L4A AGBD, with 0.1 and 0.28 higher R^2, 2.48 and 3.87 Mg/ha lower absolute MSD, and 1.87 Mg/ha and 4.77 Mg/ha lower RMSE (Fig. 11). $AGBD_{SAS\_RF}$ showed the highest model improvement compared to $AGBD_{L4A}$, with a 26% lower %RMSE and 0.28 higher R^2.

The superior performance of local models could be attributed to a number of factors, such as the inclusion of multiple GEDI metrics in the $AGBD_{SAS\_GLM}$ and $AGBD_{SAS\_RF}$ models compared to the single RH98 used in $AGBD_{L4A}$. In the case of $AGBD_{SAS\_GLM}$, GEDI RH50, RH98 and FHD were used as predictors. As a comparison to L4A, we also tested GLM using only RH98 and found that the R^2 reduced significantly from 0.71 to 0.55, suggesting that the additional GEDI metrics leads to substantial improvement in predicting AGBD. Another important difference between the local models and L4A was the fact that GEDI L4A models used

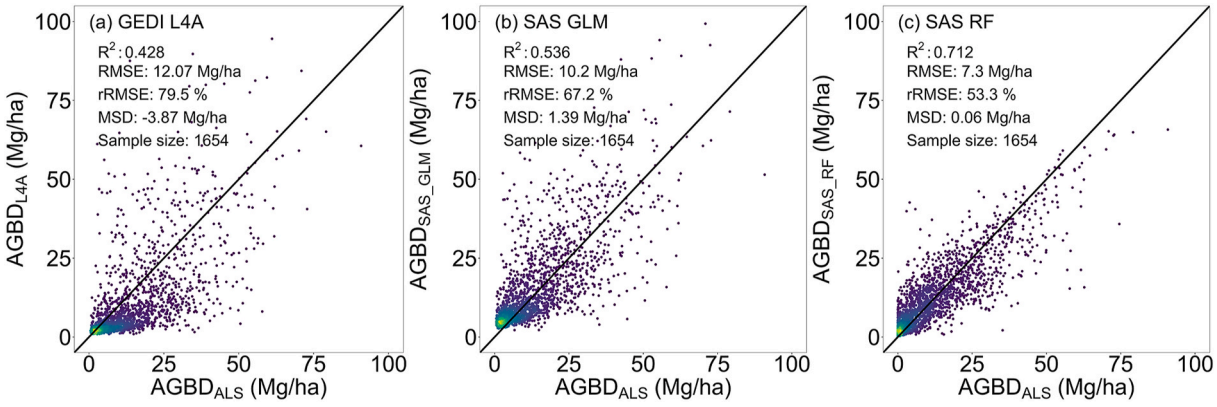

Fig. 11. Scatterplot of GEDI AGBD estimates a: $AGBD_{L4A}$; b: local $AGBD_{SAS\_GLM}$; c: local $AGBD_{SAS\_RF}$ vs. $AGBD_{ALS\_area\_MCH\_CC}$.

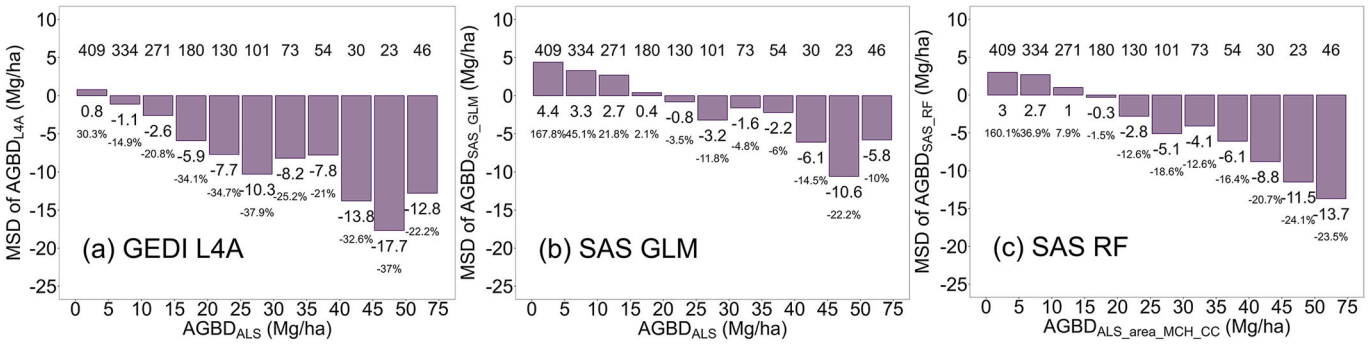

Fig. 12. The Mean Systematic Deviation (MSD) and the Relative Mean Systematic Deviation (RMSD) histogram of GEDI AGBD (a: GEDI L4A AGBD ($AGBD_{L4A}$); b: local GEDI using generalized linear model ($AGBD_{SAS\_GLM}$); c: local GEDI using Random Forest ($AGBD_{SAS\_RF}$)) vs. ALS-based AGBD (MCH × CC) ($AGBD_{ALS\_area\_MCH\_CC}$). AGBD values were grouped by bins between 0 and 50 Mg/ha at 5 Mg/ha increments, representing more than 98.5% of the total data points. The top row of numbers is the bin counts. The first and second row of numbers below bars represent the MSD and RMSD of corresponding bins, respectively. Subplots (b) and (c) were based on the results of 5-fold cross-validation.

waveforms simulated from ALS, instead of actual on-orbit GEDI waveforms and metrics. There were a number of reason why L4A had to use simulated GEDI waveforms: (i) relating field data to on-orbit GEDI was problematic because most of the leaf-on training data available for L4A were collected years before the launch of GEDI (Duncanson et al., 2022), and (ii) the GEDI geolocation error added considerable uncertainty when compared to plots at the footprint-level (Roy et al., 2021). Furthermore, simulation from ALS allowed the removal of ground mode detection error from calibration L4A models, which was necessary to avoid misspecified models. Furthermore, our previous research suggested that on-orbit GEDI RH98 had a bias, with a systematic difference −0.55m found when comparing to a sample of RH98 measurements simulated from ALS in savannas (leaf-on) (Li et al., 2023). The local models, however, were calibrated with on-orbit RH98 that included any bias, while the L4A models were developed on ALS simulated RH98. Thus, it is feasible that any local bias in the on-orbit RH98 predictor variable may have contributed to the underestimation in GEDI L4A AGBD; however, the absence of southern African savanna training data in the GEDI L4A model development could be the overriding source of uncertainty in the local applicability of these generalized models (Kellner et al., 2023).

A number of recent studies have developed local footprint-level AGBD models across a variety of vegetation types with a wide range of AGBD values that were generally higher than those in the present study. Sun et al. (2022) implemented machine learning algorithms to explore the GEDI AGBD model performance using GEDI RH metrics as predictors (RH25, RH50, RH75, RH100) over temperate and tropical forests in North America (mean AGBD = ~159 Mg/ha). Their results showed a very strong relationship between observed and predicted AGBD (R^2 = 0.82, RMSE = 19.1 Mg/ha, %RMSE = ~12%). Xu et al. (2023) developed RF models for predicting AGB using GEDI L2A (RH100) and L2B (PAI, FHD, CC_{GEDI}, etc.) metrics as predictors and field AGB samples in Shangri-La City, China (mean AGBD ~111 Mg/ha). Their results suggested a very strong relationship with an R^2 = 0.91, RMSE = 19.7 Mg/ha and %RMSE = ~17.2%. Bullock et al. (2023) developed local AGBD models using on-orbit GEDI RH5, RH45, RH91 and field surveys from Paraguay's national forest inventory (NFI) for five different forest types (humid forests, subhumid Cerrado forests, subhumid flooded forests, Chaco dry forests, and palm forests) (mean ABGD = 73.1 Mg/ha, AGBD range = 34.2 Mg/ha - 111.4 Mg/ha). The validation results of this country-wide locally calibrated AGBD model yielded an RMSE of 33.5 Mg/ha (%RMSE = 51.1%) and an R^2 of 0.59. Dorado-Roda et al. (2021) developed locally calibrated GEDI AGB models using ALS-based AGB estimates and on-orbit GEDI metrics (RH0-100, PAI, FHD, CC_{GEDI}) in Spain for a wide range of forest ecosystems. When considering only the lowest biomass uneven-aged sparse oak forest with a mean AGBD of 28.25 Mg/ha, the results yielded an RMSE of 14.5 Mg/ha and %RMSE of 51.4%. Jia et al. (2024) assessed the accuracy of GEDI L4A using National Ecological Observatory Network (NEON) during 2018–2019 across the continental USA. The results from lower biomass sites (AGBD <150 Mg/ha) yielded R^2 between 0.43 and 0.73 and %RMSEs between 55.8% and 63%. A recent study by Leite et al. (2022) in the Brazilian Cerrado/tropical savannas present the only results within a biomass range (mean AGBD = 13.9 Mg/ha) that is comparable to the current study in low biomass savannas. They used GEDI data to estimate woody fuel load based on multiple GEDI L2A and L2B metrics (RH98, PAI, FHD, and CC_{GEDI}) using an RF model with accurate AGBD estimations (R^2 = 0.71, RMSE = 23 Mg/ha, %RMSE = 40.7%), which were very similar to our RF-based results in southern African savannas (R^2 = 0.71, RMSE = 7.3 Mg/ha, %RMSE = 53.3%). While the non-parametric RF is known for its flexibility and generalization capability and achieved the best model performance in our study (R^2 = 0.71, RMSE = 7.3 Mg/ha), there are several caveats to keep in mind when extending the model to a larger area, such as, differences in data distributions, training data representativeness, and changes in allometric relationships in different savanna vegetation types (Chave et al., 2005; Colgan et al., 2013). Most importantly, the RF model is prone to overfitting to the local data with an unknown generalization over larger complex and heterogeneous regions (Lu et al., 2016).

Investigating the MSD distribution within specific AGBD bins provides useful insight into under and overestimations across the range of AGBD values. $AGBD_{L4A}$ underestimated significantly, especially in the 15–50 Mg/ha bins with RMSD of −21% to −37.9%, while the local models ($AGBD_{SAS\_GLM}$ and $AGBD_{SAS\_RF}$) underestimated by much less (−1.5% to −24.1%) in this range (Fig. 12). The local model using GLM was therefore most accurate, with a negative MSD remaining < −10.6 Mg/ha or −22.2%, up to 50 Mg/ha (Fig. 12), which represents a very large portion of AGBD variation in southern African savannas (Fig. 9). $AGBD_{SAS\_GLM}$ and $AGBD_{SAS\_RF}$ underestimated with a mean of −3.4 Mg/ha (−8.6%) and −5.5 Mg/ha (−15.2%) respectively for the bins between 15 and 50 Mg/ha, while $AGBD_{L4A}$ exceeded 20% underestimation for almost all bins above 10 Mg/ha. The underestimation of the local models stabilized at high AGBD levels (50–75 Mg/ha) with RMSD of 10–23%. The $AGBD_{SAS\_GLM}$ provided the lowest mean RMSD of 9.2% across the range of bins above 10 Mg/ha, which was consistently about half that of $AGBD_{SAS\_RF}$ especially in the 20–40 Mg/ha range (Fig. 12 b, c).

Overall, the study demonstrated that local models achieved higher accuracy using local ALS data products and field measured AGBD than the broadly trained GSW $AGBD_{L4A}$ model. This should be expected given that the local models were based on a single tree allometric model, consistent field data collection protocols and contemporaneous ALS data collection, while the GEDI L4A AGBD approach used multiple allometry models and diverse field data protocols. Furthermore, the GEDI L4A modeling process was based on GEDI RH metrics simulated from ALS

data, while the local models were based on collocated, observed GEDI metrics. This highlights the importance and benefits of local calibration of biomass models to unlock the full potential of GEDI metrics for estimating AGBD (Bruening et al., 2023; Bullock et al., 2023; Pascual et al., 2023). The local $AGBD_{SAS}$ models are representative of a diversity of the vegetation types including fine and broadleaf vegetation, (specifically Southern African Bushveld and Zambezian Mopane woodlands ecoregions (Dinerstein et al., 2017)), with a wide mean annual precipitation (MAP) range of 350–750 mm and AGBD range of 0–50 Mg/ha. Although our AGBD models were calibrated with a few data points (1.4%) with AGBD >50 Mg/ha (Figs. 11 and 12), these are not sufficient to ensure that the models are applicable to, e.g., wet (>1000 mm MAP) Eastern Miombo woodlands with AGBD of 90 Mg/ha (Chidumayo, 1991; Desanker et al., 1997; Guy, 1981) (Fig. 9). This echoes the ever-present trade-off between locally specific models that fit the data well and regional models that generalize well over large areas (Eisfelder et al., 2012; McRoberts et al., 2019a, 2019b). Fortunately, more AGBD field data are becoming available for expanded model calibration, e.g. via the Socio-Ecological Observatory for Studying African Woodlands (SEOSAW) networks which have collected data at more than 120 1ha field plots (25% of these with ALS or drone LiDAR data) in southern Africa (The SEOSAW partnership, 2021). The field and ALS data used in the present study have subsequently been contributed to the GEDI Forest Structure and Biomass Database (FSBD) and will be included in the reference data for future versions of GEDI L4A AGBD data product (Duncanson et al., 2022; Kellner et al., 2023).

One of the primary objectives of the GEDI mission is to deliver a 1-km gridded product (L4B) with a standard error amounting to 20% of the mean AGBD within at least 80% of 1-km cells. Continued improvement of the GEDI footprint-level AGBD estimates ultimately leads to improvement in the GEDI L4B AGBD gridded product, which uses hybrid inference to aggregate L4A estimates (25 m) into 1-km cells (Patterson et al., 2019). The GEDI L4B estimates can otherwise be aggregated to derive mean and uncertainty values at various scales, ranging from specific regions to entire countries. Accurate footprint-level GEDI AGBD data will also serve as essential reference data for developing the AGBD products using the L-band SAR data from the imminent NISAR mission (NISAR, 2018).

AGBD predictions across large areas using, e.g. SAR imagery, contain uncertainty due to multiple sources of error in field measurements, allometry, sampling and modeling (Phillips et al., 2000; Urbazaev et al., 2018). Uncertainty in each stage of the estimation process contributes to the total uncertainty, and ignoring error sources from one stage can potentially lead to substantial underestimation of uncertainty of the final SAR-based AGBD estimation (Bouvet et al., 2018; Coops et al., 2021; Duncanson et al., 2021; Urbazaev et al., 2018). It should therefore be recognized that the model parameter error from the field to ALS biomass model in the present study was not propagated to the ALS AGBD, which in turn was used as reference data in the footprint-level GEDI AGB models. We assumed that the field plots used to develop ALS AGBD models were well specified and "design unbiased" (Ståhl et al., 2024), and applicable to the population to which they were being applied. Working within constraints imposed by the available field data, we ensured that the field to ALS model was an unbiased predictor of the true AGBD; however, ignoring the uncertainty contributed by this model in large area estimation (e.g. Dubayah et al. (2022) would lead to over-optimistic estimates of precision (Saarela et al., 2018). The parametric modeling of AGBD from field to ALS to GEDI and ultimately, to SAR, will enable the fusion of GEDI and SAR to produce savanna AGBD maps, along with realistic estimates of uncertainty from statistical inference frameworks, such as Generalized Hierarchical Model-Based (GHMB) inference (Saarela et al., 2016, 2018, 2022).

5. Conclusion

GEDI is a pioneering mission explicitly designed to measure vegetation structures, with its statistical estimation framework integrated into its mission design (Dubayah et al., 2022). The generation of regional to global gridded biomass maps from GEDI relies on accurate footprint-level AGBD estimates. However, the current GEDI L4A models use simulated RH metrics and the global reference dataset that contains unavoidable geographic gaps. Given that African savannas were underrepresented in the reference data, the GEDI biomass products can greatly benefit from the development of more accurate footprint-level AGBD models that use on-orbit GEDI L2A and L2B metrics and additional field and ALS reference data. The local GEDI AGBD results using GLM and RF outperformed GEDI L4A AGBD with higher R^2 and significantly smaller error measures. The local GEDI AGBD using RF had the highest R^2 of 0.71 and lowest % RMSE of 53.3%, while the GLM results provided the lowest RMSD of 9.2% (Fig. 12), which was half that of RF results across the range of bins above 10 Mg/ha. Local GEDI AGBD estimates based on multiple on-orbit GEDI metrics were more reliable than GEDI L4A product that currently uses a global GSW model to predict AGBD as a function of simulated RH98. The field and ALS data used in the present study have subsequently been contributed to the GEDI FSBD (Duncanson et al., 2022) and will be included in future versions of GEDI L4A AGBD data product. This research paves the way for the integration of the local GEDI AGBD estimates with spatially complete remote sensing data (e.g. NISAR, ALOS-2 PALSAR-2) to derive large-scale biomass products for monitoring changes in savanna carbon stocks due to multiple drivers and management interventions (Asner et al., 2016; Skole et al., 2021; Smit et al., 2016; Smit and Prins, 2015; Wessels et al., 2023).

Funding

The research was funded by NASA Carbon Monitoring System (Grant number 80NSSC21K0967) (United States). The CSIR Strategic Research Panel (South Africa) funded the ALS and field data collection. XL was supported by a George Mason University Presidential Scholarship (United States). The funding sources were not directly involved in the research.

Data availability

The GEDI Level-2A, Level-2B and Level-4A data are available from the NASA LPDAAC. The authors do not have permission to share the field and airborne LiDAR data used in this study.

CRediT authorship contribution statement

Xiaoxuan Li: Writing – review & editing, Writing – original draft, Visualization, Validation, Software, Resources, Project administration, Methodology, Formal analysis. **Konrad Wessels:** Writing – review & editing, Writing – original draft, Supervision, Project administration, Methodology, Investigation, Funding acquisition, Conceptualization. **John Armston:** Writing – review & editing, Methodology, Investigation, Funding acquisition, Conceptualization. **Laura Duncanson:** Writing – review & editing, Methodology, Conceptualization. **Mikhail Urbazaev:** Writing – review & editing, Software, Resources. **Laven Naidoo:** Writing – review & editing, Resources, Methodology, Formal analysis, Data curation. **Renaud Mathieu:** Writing – review & editing, Funding acquisition, Conceptualization. **Russell Main:** Writing – review & editing, Resources, Methodology, Formal analysis, Data curation.

Declaration of competing interest

The authors declare that they have no known competing financial interests or personal relationships that could have appeared to influence the work reported in this paper.

Data availability

The authors do not have permission to share data.

Acknowledgements

The South African Environmental Observation Network (SAEON), Ndlovo node, in particular Mightyman Mashele and Dr. Tony Swemmer, played a key role in collecting the field data. The DeBeers Group allowed field work in the Venetia-Limpopo Reserve. The CSIR and University of Witwatersrand agreed to the use of the field and ALS data they acquired.

Appendix 1. The correlation and values for each pair of GEDI metrics in the GLM model selection

Combination of predictors in GLMs	R^2 of predicted vs. reference AGBD	VIF of predictor pairs	Correlation coefficient of predictor pairs
RH98	0.41	N/A	
RH75	0.42	N/A	
RH50	0.3	N/A	
Cover	0.37	N/A	
FHD	0.24	N/A	
PAI	0.35	N/A	RH98+Cover: 0.75
RH98+RH50	0.46	RH98: 1.4, RH50: 1.4	RH98+FHD: 0.81
RH98+Cover	0.45	RH98: 2.3, Cover: 2.3	RH98+PAI: 0.71
RH98+FHD	0.42	RH98: 2.9, FHD: 2.9	RH98+RH50: 0.6
RH98+PAI	0.45	RH98: 2, FHD: 2	RH50+Cover: 0.8
RH98+RH50+Cover	0.46	RH98: 4.2, RH50: 2.8, Cover: 2.3	RH50+FHD: 0.37
RH98+RH50+PAI	0.46	RH98: 4.9, RH50: 3.7, PAI: 2	RH50+PAI: 0.85
RH98+RH50+FHD	**0.47**	**RH98: 2.6, RH50: 5.3, FHD: 4.1**	RH98+RH75: 0.78
RH98+RH75+Cover	0.47	RH98: 2.7, RH75: 5, Cover: 4.4	RH75+Cover: 0.87
RH98+RH75+PAI	0.47	RH98: 6, RH75: 2.8, PAI: 3.2	RH75+FHD: 0.54
RH98+RH75+FHD	0.47	RH98: 6, RH75: 2.8, FHD: 3.2	RH75+PAI: 0.86
RH98+Cover + FHD	0.45	RH98: 4.8, Cover: 2.3, FHD: 3	Cover + FHD:0.56
RH98+Cover + PAI	0.45	RH98: 4.8, Cover: 2.3, PAI: 3	Cover + PAI: 0.97
RH98+PAI + FHD	0.45	RH98: 4.5, PAI: 2, FHD: 3	FHD + PAI: 0.51

References

Archibald, S., Scholes, R.J., 2007. Leaf green-up in a semi-arid African savanna - separating tree and grass responses to environmental cues. J. Veg. Sci. 18, 583–594.

Ashton, M.S., Tyrrell, M.L., Spalding, D., Gentry, B., 2012. Managing Forest Carbon in a Changing Climate. Springer Science & Business Media.

Asner, G.P., Mascaro, J., 2014. Mapping tropical forest carbon: calibrating plot estimates to a simple LiDAR metric. Remote Sensing of Environment 140, 614–624. https://doi.org/10.1016/j.rse.2013.09.023.

Asner, G.P., Mascaro, J., Muller-Landau, H.C., Vieilledent, G., Vaudry, R., Rasamoelina, M., Hall, J.S., van Breugel, M., 2012. A universal airborne LiDAR approach for tropical forest carbon mapping. Oecologia 168, 1147–1160. https://doi.org/10.1007/s00442-011-2165-z.

Asner, G.P., Vaughn, N., Smit, I.P.J., Levick, S., 2016. Ecosystem-scale effects of megafauna in African savannas. Ecography 39, 240–252. https://doi.org/10.1111/ecog.01640.

Atmani, F., Bookhagen, B., Smith, T., 2022. Measuring vegetation heights and their seasonal changes in the western Namibian savanna using spaceborne lidars. Rem. Sens. 14, 2928. https://doi.org/10.3390/rs14122928.

Bastin, J.-F., Berrahmouni, N., Grainger, A., Maniatis, D., Mollicone, D., Moore, R., Patriarca, C., Picard, N., Sparrow, B., Abraham, E.M., Aloui, K., Atesoglu, A., Attore, F., Bassüllü, Ç., Bey, A., Garzuglia, M., García-Montero, L.G., Groot, N., Guerin, G., Laestadius, L., Lowe, A.J., Mamane, B., Marchi, G., Patterson, P., Rezende, M., Ricci, S., Salcedo, I., Diaz, A.S.-P., Stolle, F., Surappaeva, V., Castro, R., 2017. The extent of forest in dryland biomes. Science 356, 635–638. https://doi.org/10.1126/science.aam6527.

Beck, J., Armston, J., Hofton, M., Luthcke, S., 2021. Global ecosystem dynamics investigation (GEDI) level 02 user guide. In: Sioux Falls, South Dakota, USA: EROS Center, US Geological Survey.

Bergen, K.M., Goetz, S.J., Dubayah, R.O., Henebry, G.M., Hunsaker, C.T., Imhoff, M.L., Nelson, R.F., Parker, G.G., Radeloff, V.C., 2009. Remote sensing of vegetation 3-D structure for biodiversity and habitat: review and implications for lidar and radar spaceborne missions. J. Geophys. Res.: Biogeosciences 114.

Blair, J.B., Hofton, M.A., 1999. Modeling laser altimeter return waveforms over complex vegetation using high-resolution elevation data. Geophys. Res. Lett. 26, 2509–2512. https://doi.org/10.1029/1999GL010484.

Bombelli, A., Avitabile, V., Balzter, H., Marchesini, L.B., Bernoux, M., Brady, M., Hall, R., Hansen, M., Henry, M., Herold, M., 2009. Biomass—assessment of the status of the development of the standards for the terrestrial essential climate variables. Rome. GTOS 18.

Bouvet, A., Mermoz, S., Le Toan, T., Villard, L., Mathieu, R., Naidoo, L., Asner, G.P., 2018. An above-ground biomass map of African savannahs and woodlands at 25m resolution derived from ALOS PALSAR. Remote Sens. Environ. 206, 156–173.

Breiman, L., 2001. Random forests. Mach. Learn. 45, 5–32.

Bruening, J.M., May, P.B., Armston, J.D., Dubayah, R.O., 2023. Precise and unbiased biomass estimation from GEDI data and the US forest inventory. Frontiers in Forests and Global Change 6, 1149153.

Bullock, E.L., Healey, S.P., Yang, Z., Acosta, R., Villalba, H., Insfrán, K.P., Melo, J.B., Wilson, S., Duncanson, L., Næsset, E., Armston, J., Saarela, S., Ståhl, G., Patterson, P. L., Dubayah, R., 2023. Estimating aboveground biomass density using hybrid statistical inference with GEDI lidar data and Paraguay's national forest inventory. Environ. Res. Lett. 18, 085001 https://doi.org/10.1088/1748-9326/acdf03.

Camarretta, N., Harrison, P.A., Bailey, T., Potts, B., Lucieer, A., Davidson, N., Hunt, M., 2019. Monitoring forest structure to guide adaptive management of forest restoration: a review of remote sensing approaches. N. For. https://doi.org/10.1007/s11056-019-09754-5.

Chave, J., Andalo, C., Brown, S., Cairns, M.A., Chambers, J.Q., Eamus, D., Fölster, H., Fromard, F., Higuchi, N., Kira, T., 2005. Tree allometry and improved estimation of carbon stocks and balance in tropical forests. Oecologia 145, 87–99.

Chidumayo, E.N., 1991. Seedling development of the miombo woodland tree Julbernardia globiflora. J. Veg. Sci. 2, 21–26.

Colgan, M.S., Asner, G.P., Levick, S.R., Martin, R.E., Chadwick, O.A., 2012. Topo-edaphic controls over woody plant biomass in South African savannas. Biogeosciences 9, 1809–1821. https://doi.org/10.5194/bg-9-1809-2012.

Colgan, M.S., Asner, G.P., Swemmer, T., 2013. Harvesting tree biomass at the stand level to assess the accuracy of field and airborne biomass estimation in savannas. Ecol. Appl. 23, 1170–1184. https://doi.org/10.1890/12-0922.1.

Coomes, D.A., Dalponte, M., Jucker, T., Asner, G.P., Banin, L.F., Burslem, D.F.R.P., Lewis, S.L., Nilus, R., Phillips, O.L., Phua, M.-H., Qie, L., 2017. Area-based vs tree-centric approaches to mapping forest carbon in Southeast Asian forests from airborne laser scanning data. Remote Sensing of Environment 194, 77–88. https://doi.org/10.1016/j.rse.2017.03.017.

Coops, N.C., Tompalski, P., Goodbody, T.R.H., Queinnec, M., Luther, J.E., Bolton, D.K., White, J.C., Wulder, M.A., van Lier, O.R., Hermosilla, T., 2021. Modelling lidar-derived estimates of forest attributes over space and time: a review of approaches and future trends. Remote Sensing of Environment 260, 112477. https://doi.org/10.1016/j.rse.2021.112477.

Dalponte, M., Coomes, D.A., 2016. Tree-centric mapping of forest carbon density from airborne laser scanning and hyperspectral data. Methods Ecol. Evol. 7, 1236–1245. https://doi.org/10.1111/2041-210X.12575.

Davies, A.B., Asner, G.P., 2019. Elephants limit aboveground carbon gains in African savannas. Global Change Biol. 25, 1368–1382. https://doi.org/10.1111/gcb.14585.

Davies, A.B., Gaylard, A., Asner, G.P., 2018. Megafaunal effects on vegetation structure throughout a densely wooded African landscape. Ecol. Appl. 28, 398–408. https://doi.org/10.1002/eap.1655.

Dayaram, A., Harris, L.R., Grobler, B.A., Merwe, S. van der, Rebelo, A.G., Powrie, L.W., Vlok, J.H.J., Desmet, P.G., Qabaqaba, M., Hlahane, K.M., Skowno, A.L., 2019.

Vegetation Map of South Africa, Lesotho and Swaziland 2018: a description of changes since 2006. Bothalia 49, 11. https://doi.org/10.4102/abc.v49i1.2452.
Desanker, P.V., Frost, P.G.H., Justice, C.O., Scholes, R.J., 1997. The Miombo network: framework for a terrestrial transect study of land-use and land-cover change in the Miombo ecosystems of Central Africa: conclusions of the Miombo network Workshop, Zomba, Malawi, December 1995. Global Change Report (Sweden).
Dinerstein, E., Olson, D., Joshi, A., Vynne, C., Burgess, N.D., Wikramanayake, E., Hahn, N., Palminteri, S., Hedao, P., Noss, R., 2017. An ecoregion-based approach to protecting half the terrestrial realm. Bioscience 67, 534–545.
Dorado-Roda, I., Pascual, A., Godinho, S., Silva, C.A., Botequim, B., Rodríguez-Gonzálvez, P., González-Ferreiro, E., Guerra-Hernández, J., 2021. Assessing the accuracy of GEDI data for canopy height and aboveground biomass estimates in Mediterranean forests. Rem. Sens. 13, 2279.
Drake, J.B., Dubayah, R.O., Knox, R.G., Clark, D.B., Blair, J.B., 2002. Sensitivity of large-footprint lidar to canopy structure and biomass in a neotropical rainforest. Remote Sensing of Environment 81, 378–392. https://doi.org/10.1016/S0034-4257(02)00013-5.
Dubayah, R., Armston, J., Healey, S.P., Bruening, J.M., Patterson, P.L., Kellner, J.R., Duncanson, L., Saarela, S., Ståhl, G., Yang, Z., Tang, H., Blair, J.B., Fatoyinbo, L., Goetz, S., Hancock, S., Hansen, M., Hofton, M., Hurtt, G., Luthcke, S., 2022. GEDI launches a new era of biomass inference from space. Environ. Res. Lett. 17, 095001 https://doi.org/10.1088/1748-9326/ac8694.
Dubayah, R., Armston, J., Kellner, J., Duncanson, L., Healey, S., Patterson, P., Hancock, S., Tang, H., Hofton, M., Blair, B., Luthcke, S., 2021a. GEDI L4A Footprint Level Aboveground Biomass Density, Version 1. ORNL DAAC, Oak Ridge, Tennessee, USA. https://doi.org/10.3334/ORNLDAAC/1907.
Dubayah, R., Blair, J.B., Goetz, S., Fatoyinbo, L., Hansen, M., Healey, S., Hofton, M., Hurtt, G., Kellner, J., Luthcke, S., Armston, J., Tang, H., Duncanson, L., Hancock, S., Jantz, P., Marselis, S., Patterson, P.L., Qi, W., Silva, C., 2020a. The global ecosystem dynamics investigation: high-resolution laser ranging of the Earth's forests and topography. Science of Remote Sensing 1, 100002. https://doi.org/10.1016/j.srs.2020.100002.
Dubayah, R., Hofton, M., Blair, B., Armston, J., Tang, H., Luthcke, S., 2021b. GEDI L2A elevation and height metrics data global footprint level V002. NASA EOSDIS Land Processes Distributed Active Archive Center. https://doi.org/10.5067/GEDI/GEDI02_A.002 [Data set].
Dubayah, R., Luthcke, S., Blair, B., Hofton, M., Armston, J., Tang, H., 2020b. GEDI L1B geolocated waveform data global footprint level V002 [data set]. NASA EOSDIS Land Processes Distributed Active Archive Center. https://doi.org/10.5067/GEDI/GEDI01_B.002.
Dubayah, R., Tang, H., Armston, J., Luthcke, S., Hofton, M., Blair, B., 2021c. GEDI L2B canopy cover and vertical profile metrics data global footprint level V002. NASA EOSDIS Land Processes Distributed Active Archive Center. https://doi.org/10.5067/GEDI/GEDI02_B.002 [Data set].
Dubayah, R.O., Drake, J.B., 2000. Lidar remote sensing for forestry. J. For. 98, 44–46. https://doi.org/10.1093/jof/98.6.44.
Duncanson, L., Armston, J., Disney, M., Avitabile, V., Barbier, N., Calders, K., Carter, S., Chave, J., Herold, M., Crowther, T.W., Falkowski, M., Kellner, J.R., Labrière, N., Lucas, R., MacBean, N., McRoberts, R.E., Meyer, V., Næsset, E., Nickeson, J.E., Paul, K.I., Phillips, O.L., Réjou-Méchain, M., Román, M., Roxburgh, S., Saatchi, S., Schepaschenko, D., Scipal, K., Siqueira, P.R., Whitehurst, A., Williams, M., 2019. The importance of consistent global forest aboveground biomass product validation. Surv. Geophys. 40, 979–999. https://doi.org/10.1007/s10712-019-09538-8.
Duncanson, L., Armston, J., Disney, M., Avitabile, V., Barbier, N., Calders, K., Carter, S., Chave, J., Herold, M., MacBean, N., McRoberts, R., Minor, D., Paul, K., Réjou-Méchain, M., Roxburgh, S., Williams, M., Albinet, C., Baker, T., Bartholomeus, H., Bastin, J.F., Coomes, D., Crowther, T., Davies, S., de Bruin, S., De Kauwe, M., Domke, G., Dubayah, R., Falkowski, M., Fatoyinbo, L., Goetz, S., Jantz, P., Jonckheere, I., Jucker, T., Kay, H., Kellner, J., Labrière, N., Lucas, R., Mitchard, E., Morsdorf, F., Næsset, E., Park, T., Phillips, O.L., Ploton, P., Puliti, S., Guegan, S., Saatchi, S., Schaaf, C., Schepaschenko, D., Scipal, K., Stovall, A., Thiel, C., Wulder, M.A., Camacho, F., Nickeson, J., Román, M., Margolis, H., 2021. In: Aboveground Woody Biomass Product Validation Good Practices Protocol. https://doi.org/10.5067/doc/ceoswgcv/lpv/agb.001.
Duncanson, L., Kellner, J.R., Armston, J., Dubayah, R., Minor, D.M., Hancock, S., Healey, S.P., Patterson, P.L., Saarela, S., Marselis, S., Silva, C.E., Bruening, J., Goetz, S.J., Tang, H., Hofton, M., Blair, B., Luthcke, S., Fatoyinbo, L., Abernethy, K., Alonso, A., Andersen, H.-E., Aplin, P., Baker, T.R., Barbier, N., Bastin, J.F., Biber, P., Boeckx, P., Bogaert, J., Boschetti, L., Boucher, P.B., Boyd, D.S., Burslem, D.F.R.P., Calvo-Rodriguez, S., Chave, J., Chazdon, R.L., Clark, D.B., Clark, D.A., Cohen, W.B., Coomes, D.A., Corona, P., Cushman, K.C., Cutler, M.E.J., Dalling, J.W., Dalponte, M., Dash, J., de-Miguel, S., Deng, S., Ellis, P.W., Erasmus, B., Fekety, P.A., Fernandez-Landa, A., Ferraz, A., Fischer, R., Fisher, A.G., García-Abril, A., Gobakken, T., Hacker, J.M., Heurich, M., Hill, R.A., Hopkinson, C., Huang, H., Hubbell, S.P., Hudak, A.T., Huth, A., Imbach, B., Jeffery, K.J., Katoh, M., Kearsley, E., Kenfack, D., Kljun, N., Knapp, N., Král, K., Krůček, M., Labrière, N., Lewis, S.L., Longo, M., Lucas, R.M., Main, R., Manzanera, J.A., Martínez, R.V., Mathieu, R., Memiaghe, H., Meyer, V., Mendoza, A.M., Monerris, A., Montesano, P., Morsdorf, F., Næsset, E., Naidoo, L., Nilus, R., O'Brien, M., Orwig, D.A., Papathanassiou, K., Parker, G., Philipson, C., Phillips, O.L., Pisek, J., Poulsen, J.R., Pretzsch, H., Rüdiger, C., Saatchi, S., Sanchez-Azofeifa, A., Sanchez-Lopez, N., Scholes, R., Silva, C.A., Simard, M., Skidmore, A., Stereńczak, K., Tanase, M., Torresan, C., Valbuena, R., Verbeeck, H., Vrska, T., Wessels, K., White, J.C., White, L.J.T., Zahabu, E., Zgraggen, C., 2022. Aboveground biomass density models for NASA's Global Ecosystem Dynamics Investigation (GEDI) lidar mission. Remote Sensing of Environment 270, 112845. https://doi.org/10.1016/j.rse.2021.112845.
Duncanson, L.I., Cook, B.D., Hurtt, G.C., Dubayah, R.O., 2014. An efficient, multi-layered crown delineation algorithm for mapping individual tree structure across multiple ecosystems. Remote Sensing of Environment 154, 378–386. https://doi.org/10.1016/j.rse.2013.07.044.
Duncanson, L.I., Dubayah, R.O., Cook, B.D., Rosette, J., Parker, G., 2015. The importance of spatial detail: assessing the utility of individual crown information and scaling approaches for lidar-based biomass density estimation. Remote Sensing of Environment 168, 102–112. https://doi.org/10.1016/j.rse.2015.06.021.
Eisfelder, C., Kuenzer, C., Dech, S., 2012. Derivation of biomass information for semi-arid areas using remote-sensing data. Int. J. Rem. Sens. 33, 2937–2984.
FAO, 2012. Global Ecological Zones for FAO Forest Reporting: 2010 Update. FAO, Rome, Italy.
Fatoyinbo, T., Armston, J., Simard, M., Saatchi, S., Denbina, M., Lavalle, M., Hofton, M., Tang, H., Marselis, S., Pinto, N., Hancock, S., Hawkins, B., Duncanson, L., Blair, B., Hansen, C., Lou, Y., Dubayah, R., Hensley, S., Silva, C., Poulsen, J.R., Labrière, N., Barbier, N., Jeffery, K., Kenfack, D., Herve, M., Bissiengou, P., Alonso, A., Moussavou, G., White, L.T.J., Lewis, S., Hibbard, K., 2021. The NASA AfriSAR campaign: airborne SAR and lidar measurements of tropical forest structure and biomass in support of current and future space missions. Remote Sensing of Environment 264, 112533. https://doi.org/10.1016/j.rse.2021.112533.
Ferraz, A., Saatchi, S., Mallet, C., Jacquemoud, S., Gonçalves, G., Silva, C.A., Soares, P., Tomé, M., Pereira, L., 2016a. Airborne lidar estimation of aboveground forest biomass in the absence of field inventory. Rem. Sens. 8, 653.
Ferraz, A., Saatchi, S., Mallet, C., Meyer, V., 2016b. Lidar detection of individual tree size in tropical forests. Remote Sensing of Environment 183, 318–333.
Guy, P.R., 1981. Changes in the biomass and productivity of woodlands in the sengwa wildlife research area, Zimbabwe. J. Appl. Ecol. 507–519.
Hanan, N.P., Prihodko, L., Ross, C.W., Bucini, G., Tredennick, A.T., 2020. Gridded Estimates of Woody Cover and Biomass across Sub-saharan Africa, 2000-2004. ORNL DAAC.
Hancock, S., Armston, J., Hofton, M., Sun, X., Tang, H., Duncanson, L.I., Kellner, J.R., Dubayah, R., 2019. The GEDI simulator: a large-footprint waveform lidar simulator for calibration and validation of spaceborne missions. Earth Space Sci. 6, 294–310. https://doi.org/10.1029/2018EA000506.
Herold, M., Carter, S., Avitabile, V., Espejo, A.B., Jonckheere, I., Lucas, R., McRoberts, R. E., Næsset, E., Nightingale, J., Petersen, R., Reiche, J., Romijn, E., Rosenqvist, A., Rozendaal, D.M.A., Seifert, F.M., Sanz, M.J., De Sy, V., 2019. The role and need for space-based forest biomass-related measurements in environmental management and policy. Surv. Geophys. 40, 757–778. https://doi.org/10.1007/s10712-019-09510-6.
Hofton, M., Blair, J.B., 2020. Algorithm theoretical basis document (ATBD) for GEDI transmit and receive waveform processing for L1 and L2 products 44. https://lpdaac.usgs.gov/documents/581/GEDI_WF_ATBD_v1.0.pdf.
Hofton, M.A., Minster, J.B., Blair, J.B., 2000. Decomposition of laser altimeter waveforms. IEEE Trans. Geosci. Rem. Sens. 38, 1989–1996. https://doi.org/10.1109/36.851780.
Holmgren, J., Persson, Å., 2004. Identifying species of individual trees using airborne laser scanner. Remote Sensing of Environment 90, 415–423.
Jia, D., Wang, C., Hakkenberg, C.R., Numata, I., Elmore, A.J., Cochrane, M.A., 2024. Accuracy evaluation and effect factor analysis of GEDI aboveground biomass product for temperate forests in the conterminous United States. GIScience Remote Sens. 61, 2292374 https://doi.org/10.1080/15481603.2023.2292374.
Kellner, J.R., Armston, J., Duncanson, L., 2023. Algorithm theoretical basis document for GEDI footprint aboveground biomass density. Earth Space Sci. 10, e2022EA002516.
Lefsky, M.A., Cohen, W.B., Parker, G.G., Harding, D.J., 2002. Lidar remote sensing for ecosystem studies. Bioscience 52, 19–30.
Leite, R.V., Silva, C.A., Broadbent, E.N., Do Amaral, C.H., Liesenberg, V., De Almeida, D. R.A., Mohan, M., Godinho, S., Cardil, A., Hamamura, C., 2022. Large scale multi-layer fuel load characterization in tropical savanna using GEDI spaceborne lidar data. Remote Sensing of Environment 268, 112764.
Leitold, V., Keller, M., Morton, D.C., Cook, B.D., Shimabukuro, Y.E., 2015. Airborne lidar-based estimates of tropical forest structure in complex terrain: opportunities and trade-offs for REDD+. Carbon Bal. Manag. 10, 3. https://doi.org/10.1186/s13021-015-0013-x.
Li, W., Guo, Q., Jakubowski, M.K., Kelly, M., 2012. A new method for segmenting individual trees from the lidar point cloud. Photogramm. Eng. Rem. Sens. 78, 75–84.
Li, X., Wessels, K., Armston, J., Hancock, S., Mathieu, R., Main, R., Naidoo, L., Erasmus, B., Scholes, R., 2023. First validation of GEDI canopy heights in African savannas. Remote Sensing of Environment 285, 113402. https://doi.org/10.1016/j.rse.2022.113402.
Liang, M., Duncanson, L., Silva, J.A., Sedano, F., 2023. Quantifying aboveground biomass dynamics from charcoal degradation in Mozambique using GEDI Lidar and Landsat. Remote Sensing of Environment 284, 113367. https://doi.org/10.1016/j.rse.2022.113367.
Lu, D., Chen, Q., Wang, G., Liu, L., Li, G., Moran, E., 2016. A survey of remote sensing-based aboveground biomass estimation methods in forest ecosystems. International Journal of Digital Earth 9, 63–105. https://doi.org/10.1080/17538947.2014.990526.
Ma, W., Ye, X., Tu, F., Hu, F., 2023. Carat: an R package for covariate-adaptive randomization in clinical trials. J. Stat. Software 107, 1–47.
Maltamo, M., Peuhkurinen, J., Malinen, J., Vauhkonen, J., Packalén, P., Tokola, T., 2009. Predicting tree attributes and quality characteristics of Scots pine using airborne laser scanning data. Silva Fenn. 43 (3) https://doi.org/10.14214/sf.203.
Matsika, R., Erasmus, B.F.N., Twine, W., 2013. A tale of two villages: assessing the dynamics of fuelwood supply in communal landscapes within the Kruger to Canyons Biosphere in South Africa. Environ. Conserv. 40, 71–83.

McRoberts, R.E., Næsset, E., Liknes, G.C., Chen, Q., Walters, B.F., Saatchi, S., Herold, M., 2019a. Using a finer resolution biomass map to assess the accuracy of a regional, map-based estimate of forest biomass. Surv. Geophys. 40, 1001–1015.
McRoberts, R.E., Næsset, E., Saatchi, S., Liknes, G.C., Walters, B.F., Chen, Q., 2019b. Local validation of global biomass maps. Int. J. Appl. Earth Obs. Geoinf. 83, 101931.
Meyer, V., Saatchi, S.S., Chave, J., Dalling, J.W., Bohlman, S., Fricker, G.A., Robinson, C., Neumann, M., Hubbell, S., 2013. Detecting tropical forest biomass dynamics from repeated airborne lidar measurements. Biogeosciences 10, 5421–5438. https://doi.org/10.5194/bg-10-5421-2013.
Mitchell, A.L., Rosenqvist, A., Mora, B., 2017. Current remote sensing approaches to monitoring forest degradation in support of countries measurement, reporting and verification (MRV) systems for REDD+. Carbon Bal. Manag. 12, 1–22.
Mograbi, P.J., Asner, G.P., Witkowski, E.T.F., Erasmus, B.F.N., Wessels, K.J., Mathieu, R., Vaughn, N.R., 2017. Humans and elephants as treefall drivers in African savannas. Ecography 40, 1274–1284. https://doi.org/10.1111/ecog.02549.
Mograbi, P.J., Erasmus, B.F.N., Witkowski, E.T.F., Asner, G.P., Wessels, K.J., Mathieu, R., Knapp, D.E., Martin, R.E., Main, R., 2015. Biomass increases go under cover: woody vegetation dynamics in South African rangelands. PLoS One 10, e0127093. https://doi.org/10.1371/journal.pone.0127093.
Naidoo, L., Mathieu, R., Main, R., Kleynhans, W., Wessels, K., Asner, G., Leblon, B., 2015. Savannah woody structure modelling and mapping using multi-frequency (X-, C- and L-band) Synthetic Aperture Radar data. ISPRS J. Photogrammetry Remote Sens. 105, 234–250. https://doi.org/10.1016/j.isprsjprs.2015.04.007.
Naidoo, L., Mathieu, R., Main, R., Wessels, K., Asner, G.P., 2016. L-band Synthetic Aperture Radar imagery performs better than optical datasets at retrieving woody fractional cover in deciduous, dry savannahs. Int. J. Appl. Earth Obs. Geoinf. 52, 54–64.
Ni-Meister, W., 2015. Aboveground terrestrial biomass and carbon stock estimations from multisensor remote sensing. In: Land Resources Monitoring, Modeling, and Mapping with Remote Sensing. CRC Press, pp. 47–68.
NISAR, 2018. NASA-ISRO SAR (NISAR) Mission Science Users. NASA Jet Propulsion Laboratory, Handbook.
O'Connor, D., Ford, J., 2014. Increasing the effectiveness of the "Great Green Wall" as an adaptation to the effects of climate change and desertification in the Sahel. Sustainability 6, 7142–7154.
Padalia, H., Prakash, A., Watham, T., 2023. Modelling aboveground biomass of a multistage managed forest through synergistic use of Landsat-OLI, ALOS-2 L-band SAR and GEDI metrics. Ecol. Inf. 77, 102234 https://doi.org/10.1016/j.ecoinf.2023.102234.
Pascual, A., Guerra-Hernández, J., Armston, J., Minor, D.M., Duncanson, L.I., May, P.B., Kellner, J.R., Dubayah, R., 2023. Assessing the performance of NASA's GEDI L4A footprint aboveground biomass density models using National Forest Inventory and airborne laser scanning data in Mediterranean forest ecosystems. For. Ecol. Manag. 538, 120975 https://doi.org/10.1016/j.foreco.2023.120975.
Patterson, P.L., Healey, S.P., Ståhl, G., Saarela, S., Holm, S., Andersen, H.-E., Dubayah, R. O., Duncanson, L., Hancock, S., Armston, J., Kellner, J.R., Cohen, W.B., Yang, Z., 2019. Statistical properties of hybrid estimators proposed for GEDI—NASA's global ecosystem dynamics investigation. Environ. Res. Lett. 14, 065007 https://doi.org/10.1088/1748-9326/ab18df.
Phillips, D.L., Brown, S.L., Schroeder, P.E., Birdsey, R.A., 2000. Toward error analysis of large-scale forest carbon budgets. Global Ecol. Biogeogr. 9, 305–313.
Qi, W., Saarela, S., Armston, J., Ståhl, G., Dubayah, R., 2019. Forest biomass estimation over three distinct forest types using TanDEM-X InSAR data and simulated GEDI lidar data. Remote Sensing of Environment 232, 111283. https://doi.org/10.1016/j.rse.2019.111283.
Rodríguez-Veiga, P., Quegan, S., Carreiras, J., Persson, H.J., Fransson, J.E., Hoscilo, A., Ziółkowski, D., Stereńczak, K., Lohberger, S., Stängel, M., 2019. Forest biomass retrieval approaches from earth observation in different biomes. Int. J. Appl. Earth Obs. Geoinf. 77, 53–68.
Roussel, J.-R., Auty, D., De Boissieu, F., Meador, A.S., 2018. lidR: airborne LiDAR data manipulation and visualization for forestry applications. Remote Sensing of Environment 251. https://doi.org/10.1016/j.rse.2020.112061.
Roy, D.P., Kashongwe, H.B., Armston, J., 2021. The impact of geolocation uncertainty on GEDI tropical forest canopy height estimation and change monitoring. Science of Remote Sensing 4, 100024. https://doi.org/10.1016/j.srs.2021.100024.
Saarela, S., Holm, S., Grafström, A., Schnell, S., Næsset, E., Gregoire, T.G., Nelson, R.F., Ståhl, G., 2016. Hierarchical model-based inference for forest inventory utilizing three sources of information. Ann. For. Sci. 73, 895–910. https://doi.org/10.1007/s13595-016-0590-1.
Saarela, S., Holm, S., Healey, S.P., Andersen, H.-E., Petersson, H., Prentius, W., Patterson, P.L., Næsset, E., Gregoire, T.G., Ståhl, G., 2018. Generalized hierarchical model-based estimation for aboveground biomass assessment using GEDI and landsat data. Rem. Sens. 10, 1832. https://doi.org/10.3390/rs10111832.
Saarela, S., Holm, S., Healey, S.P., Patterson, P.L., Yang, Z., Andersen, H.-E., Dubayah, R. O., Qi, W., Duncanson, L.I., Armston, J.D., Gobakken, T., Næsset, E., Ekström, M., Ståhl, G., 2022. Comparing frameworks for biomass prediction for the global ecosystem dynamics investigation. Remote Sensing of Environment 278, 113074. https://doi.org/10.1016/j.rse.2022.113074.
Sankaran, M., Ratnam, J., Hanan, N., 2008. Woody cover in African savannas: the role of resources, fire and herbivory. Global Ecol. Biogeogr. 17, 236–245.
Scharlemann, J.P., Tanner, E.V., Hiederer, R., Kapos, V., 2014. Global soil carbon: understanding and managing the largest terrestrial carbon pool. Carbon Manag. 5, 81–91. https://doi.org/10.4155/cmt.13.77.
Schleich, A., Durrieu, S., Vega, C., 2023. Improving GEDI footprint geolocation using a high resolution digital elevation model. IEEE J. Sel. Top. Appl. Earth Obs. Rem. Sens. 1–19. https://doi.org/10.1109/JSTARS.2023.3298991.
Scholes, R., Archer, S., 1997. Tree-grass interactions in savannas. Annu. Rev. Ecol. Systemat. 28, 517–544.
Silva, C.A., Duncanson, L., Hancock, S., Neuenschwander, A., Thomas, N., Hofton, M., Fatoyinbo, L., Simard, M., Marshak, C.Z., Armston, J., Lutchke, S., Dubayah, R., 2021. Fusing simulated GEDI, ICESat-2 and NISAR data for regional aboveground biomass mapping. Remote Sensing of Environment 253, 112234. https://doi.org/10.1016/j.rse.2020.112234.
Silva, C.A., Hudak, A.T., Vierling, L.A., Loudermilk, E.L., O'Brien, J.J., Hiers, J.K., Jack, S.B., Gonzalez-Benecke, C., Lee, H., Falkowski, M.J., 2016. Imputation of individual longleaf pine (Pinus palustris Mill.) tree attributes from field and LiDAR data. Can. J. Rem. Sens. 42, 554–573.
Sitch, S., Friedlingstein, P., Gruber, N., Jones, S.D., Murray-Tortarolo, G., Ahlström, A., Doney, S.C., Graven, H., Heinze, C., Huntingford, C., 2015. Recent trends and drivers of regional sources and sinks of carbon dioxide. Biogeosciences 12, 653–679.
Skole, D.L., Mbow, C., Mugabowindekwe, M., Brandt, M.S., Samek, J.H., 2021. Trees outside of forests as natural climate solutions. Nat. Clim. Change 11, 1013–1016.
Smit, I.P.J., Asner, G.P., Govender, N., Kennedy-Bowdoin, T., Knapp, D.E., Jacobson, J., 2010. Effects of fire on woody vegetation structure in African savanna. Ecol. Appl. 20, 1865–1875.
Smit, I.P.J., Asner, G.P., Govender, N., Vaughn, N.R., Wilgen, B.W. van, 2016. An examination of the potential efficacy of high-intensity fires for reversing woody encroachment in savannas. J. Appl. Ecol. 53, 1623–1633. https://doi.org/10.1111/1365-2664.12738.
Smit, I.P.J., Prins, H.H.T., 2015. Predicting the effects of woody encroachment on mammal communities, grazing biomass and fire frequency in african savannas. PLoS One 10, e0137857. https://doi.org/10.1371/journal.pone.0137857.
Sothe, C., Gonsamo, A., Lourenço, R.B., Kurz, W.A., Snider, J., 2022. Spatially continuous mapping of forest canopy height in Canada by combining GEDI and ICESat-2 with PALSAR and sentinel. Rem. Sens. 14, 5158. https://doi.org/10.3390/rs14205158.
Ståhl, G., Gobakken, T., Saarela, S., Persson, H.J., Ekström, M., Healey, S.P., Yang, Z., Holmgren, J., Lindberg, E., Nyström, K., Papucci, E., Ulvdal, P., Ørka, H.O., Næsset, E., Hou, Z., Olsson, H., McRoberts, R.E., 2024. Why ecosystem characteristics predicted from remotely sensed data are unbiased and biased at the same time – and how this affects applications. Forest Ecosystems 11, 100164. https://doi.org/10.1016/j.fecs.2023.100164.
Sun, M., Cui, L., Park, J., García, M., Zhou, Y., Silva, C.A., He, L., Zhang, H., Zhao, K., 2022. Evaluation of NASA's GEDI lidar observations for estimating biomass in temperate and tropical forests. Forests 13, 1686. https://doi.org/10.3390/f13101686.
Swemmer, A.M., Mashele, M., Ndhlovu, P.D., 2019. Evidence for ecological sustainability of fuelwood harvesting at a rural village in South Africa. Reg. Environ. Change 19, 403–413. https://doi.org/10.1007/s10113-018-1402-y.
Tang, H., Armston, J., 2019. In: Algorithm Theoretical Basis Document (ATBD) for GEDI L2B Footprint Canopy Cover and Vertical Profile Metrics 39.
The SEOSAW partnership, 2021. A network to understand the changing socio-ecology of the southern African woodlands (SEOSAW): challenges, benefits, and methods. Plants People Planet 3, 249–267. https://doi.org/10.1002/ppp3.10168.
Tucker, C., Brandt, M., Hiernaux, P., Kariryaa, A., Rasmussen, K., Small, J., Igel, C., Reiner, F., Melocik, K., Meyer, J., Sinno, S., Romero, E., Glennie, E., Fitts, Y., Morin, A., Pinzon, J., McClain, D., Morin, P., Porter, C., Loeffler, S., Kergoat, L., Issoufou, B.-A., Savadogo, P., Wigneron, J.-P., Poulter, B., Ciais, P., Kaufmann, R., Myneni, R., Saatchi, S., Fensholt, R., 2023. Sub-continental-scale carbon stocks of individual trees in African drylands. Nature 615, 80–86. https://doi.org/10.1038/s41586-022-05653-6.
Twine, W.C., Holdo, R.M., 2016. Fuelwood sustainability revisited: integrating size structure and resprouting into a spatially realistic fuelshed model. J. Appl. Ecol. 53, 1766–1776.
Urbazaev, M., Thiel, C., Cremer, F., Dubayah, R., Migliavacca, M., Reichstein, M., Schmullius, C., 2018. Estimation of forest aboveground biomass and uncertainties by integration of field measurements, airborne LiDAR, and SAR and optical satellite data in Mexico. Carbon Bal. Manag. 13, 5. https://doi.org/10.1186/s13021-018-0093-5.
Venter, Z.S., Cramer, M.D., Hawkins, H.-J., 2018. Drivers of woody plant encroachment over Africa. Nat. Commun. 9, 2272. https://doi.org/10.1038/s41467-018-04616-8.
Wessels, K., Li, X., Bouvet, A., Mathieu, R., Main, R., Naidoo, L., Erasmus, B., Asner, G.P., 2023. Quantifying the sensitivity of L-Band SAR to a decade of vegetation structure changes in savannas. Remote Sensing of Environment 284, 113369. https://doi.org/10.1016/j.rse.2022.113369.
Wessels, K., Mathieu, R., Knox, N., Main, R., Naidoo, L., Steenkamp, K., 2019. Mapping and monitoring fractional woody vegetation cover in the arid savannas of Namibia using LiDAR training data, machine learning, and ALOS PALSAR data. Rem. Sens. 11, 2633.
Wessels, K.J., Colgan, M.S., Erasmus, B.F.N., Asner, G.P., Twine, W.C., Mathieu, R., van Aardt, J.A.N., Fisher, J.T., Smit, I.P.J., 2013. Unsustainable fuelwood extraction from South African savannas. Environ. Res. Lett. 8, 014007 https://doi.org/10.1088/1748-9326/8/1/014007.
Wigley, B.J., Bond, W.J., Hoffman, M.T., 2010. Thicket expansion in a South African savanna under divergent land use: local vs. global drivers? Global Change Biol. 16, 964–976. https://doi.org/10.1111/j.1365-2486.2009.02030.x.
Xu, L., Shu, Q., Fu, H., Zhou, W., Luo, S., Gao, Y., Yu, J., Guo, C., Yang, Z., Xiao, J., Wang, S., 2023. Estimation of quercus biomass in Shangri-La based on GEDI spaceborne lidar data. Forests 14, 876. https://doi.org/10.3390/f14050876.
Zhang, Y., Liu, J., Shen, W., 2022. A review of ensemble learning algorithms used in remote sensing applications. Appl. Sci. 12, 8654. https://doi.org/10.3390/app12178654.